This is to certify that the

dissertation entitled

DETERMINATION OF EFFECTIVE ELASTIC PROPERTIES
AND THERMAL RESIDUAL STRESSES
IN FIBER-REINFORCED COMPOSITES
BY THE BOUNDARY ELEMENT METHOD

presented by

Younghan Youn

has been accepted towards fulfillment
of the requirements for

Ph.D. degree in Mechanics

Nicholas J. Altiero
Major professor

Date 11/10/88

DETERMINATION OF EFFECTIVE ELASTIC PROPERTIES AND THERMAL RESIDUAL STRESSES IN FIBER-REINFORCED COMPOSITES BY THE BOUNDARY ELEMENT METHOD

By

Younghan Youn

A DISSERTATION

Submitted to

Michigan State University

in partial fullfillment of the requirements

for the degree of

DOCTOR OF PHILOSOPHY

Department of Metallurgy, Mechanics, and Materials Science

1988

ABSTRACT

DETERMINATION OF EFFECTIVE ELASTIC PROPERTIES AND THERMAL RESIDUAL STRESSES IN FIBER-REINFORCED COMPOSITES BY THE BOUNDARY ELEMENT METHOD

By

Younghan Youn

A boundary element formulation is developed for application to problems involving transverse-isotropic fiber-reinforced composites. Problems examined include determination of thermally-induced residual stresses due to the curing process and determination of effective transverse elastic properties in the presence of improper interfacial bonds.

The boundary element method is shown to be an effective technique for the study of the fiber/matrix interface provided that the method is adapted to handle a very thin interphase region. In the estimation of effective elastic moduli for improper interface-bonded materials, two models are introduced, i.e. the interphase degradation model and

the tangential displacement discontinuity model. These approaches have been incorporated into the boundary element model and representative numerical results are presented. Problems studied include a variety of fiber volume fractions, interphase volume fractions, and interfacial damage parameters.

ACKNOWLEDGMENTS

I would like to express appreciation to those who have helped and contributed to making this work a reality. This includes my advisor, Dr. Nicholas J. Altiero, for his great support, inspiration and valuable assistance through this period. I also would like to express appreciation to Dr. Ivvona Jasiuk for her priceless help and Drs. John F. Martin and David Yen, members of my guidance committee. A final note of appreciation must go to my family, my wife Younghee and my lovely daughters Marie, Miri and my parents for great support and encouragement.

Financial support of this work by the State of Michigan through its Research Excellence Fund is gratefully acknowledged.

TABLE OF CONTENTS

LIST OF TABLES

LIST OF FIGURES

CHAPTER 1

INTRODUCTION AND BACKGROUND

The primary advantage of " artificial materials ", such as composite materials, is that the thermal and mechanical behavior is controllable. In general, composite materials consist of two or more different materials that are formed from components large enough to be regarded as homogeneous continuous media. The search for materials with high specific strength and stiffness as well as good toughness has brought an enormous increase in research activity in the field of fiber-reinforced composite materials. The use of fiber-reinforced composite materials in engineering applications requires a fundamental understanding of the mechanical and thermal interactions between the fiber and matrix components as well as the effective material properties of the composite system.

These material properties can be determined experimentally by testing actual composite specimens. However, during the last two decades, increased attention has been given to methods for analytical prediction of these basic composite material properties as a function of the properties of the constituent materials and their geometrical relationship to each other. The previous predictions of the effective elastic properties have been based on the assumption of perfect

bonding between the constituents in the composite medium. However, the elastic moduli of a composite are not merely controlled by the elastic properties of the two phases. Cracks that can develop during cooling of the composite from it's fabrication temperature and cracks formed during stressing due to poor interfacial bonding lead to lower elastic moduli than are otherwise predicted.

In this dissertation, a more realistic effective transverse behavior of unidirectional fiber-reinforced composite materials will be studied. Here the effect of imperfect interfacial bonding and thermally-induced residual stresses, which build-up during the fabrication process, will be considered.

J. C. Maxwell [1] in 1873 and Lord Rayleigh [2] in 1892 introduced the notion of analytical determination of properties of composite materials. They computed the effective (or average) electrical conductivity of composites consisting of a matrix containing a certain distribution of spherical particles [3].

In the field of elasticity, the first approximation of effective elastic moduli of composite materials was postulated in 1889 by W. Voigt [4]. Voigt examined a composite material which consisted of a spherical inhomogeneity, with shear and bulk moduli μ_2 and K_2, imbedded in a matrix with moduli μ_1 and K_1. The volume fraction of the inhomogeneity was denoted by c_2 and that of the matrix by c_1 and the composite was subjected to uniform shear strain. He concluded that the effective shear and bulk moduli, $\bar{\mu}$ and $\bar{K}$, can be expressed as:

$$\bar{\mu} = c_1 \mu_1 + c_2 \mu_2$$

$$\bar{K} = c_1 K_1 + c_2 K_2. \qquad (1)$$

In 1929, Reuss [5] assumed that all of the elements of the composite material are subjected to a uniform stress equal to the average stress. According to Reuss's assumption, the effective moduli were obtained as:

$$\bar{\mu} = \left(\frac{c_1}{\mu_1} + \frac{c_2}{\mu_2} \right)^{-1}$$

$$\bar{K} = \left(\frac{c_1}{K_1} + \frac{c_2}{K_2} \right)^{-1}. \qquad (2)$$

Hill [6], in 1952, initiated the notion of bounding of the effective elastic moduli. He also showed on the basis of the classical extremum principles of elasticity that the Voigt approximation and the Reuss approximation are the upper and lower bounds, respectively, of the true effective elastic moduli.

In 1957, Eshelby [7] suggested the "equivalent inclusion" method. He examined the change in the gross elastic constants of a material when a dilute dispersion of ellipsoidal inhomogeneities is introduced into an infinite homogeneous isotropic elastic matrix, see Figure 1.1. Eshelby simulated a composite material as a homogeneous material having the same elastic moduli as those of the matrix and containing inclusions with shear eigenstrain ϵ_{12}^{*} (stress-free strain). The effective shear modulus, by Eshelby's equivalent inclusion method, can

be formulated for a spherical inclusion as:

$$\bar{\mu} = \frac{\mu_1[\mu_1+2S_{1212}(\mu_2-\mu_1)]}{1 + c_1(\mu_1-\mu_2)} \qquad (3)$$

where $S_{1212} = (4-\nu_1)/15(1-\nu_1)$ and ν_1 is Poisson's ratio of the matrix.

When the equivalent inclusion method is applied to obtain the stress disturbance of inhomogeneities, the existence of a matrix is assumed. However, the meaning of the matrix becomes rather vague when the volume fraction of the inclusion is increased, i.e. $c_1 \rightarrow 0$. Furthermore, the interaction among inhomogeneities becomes more prominent as the number of particles increases. Kröner [8] and Budiansky and Wu [9], in 1958 and 1962 respectively, proposed the self-consistent method in order to avoid this difficulty. In 1964, Hill [10] employed this technique to derive expressions for the elastic constants of aggregates of crystals. He modeled the composite as a single fiber embedded in an unbounded homogeneous medium which was macroscopically indistinguishable from the composite, i.e. of shear modulus $\bar{\mu}$ and Poisson's ratio $\bar{\nu}$, as shown in Figure 1.2. The effective shear modulus, $\bar{\mu}$ and effective bulk modulus, $\bar{K}$ can be expressed by the self-consistent method approximation as :

$$\bar{\mu} = \mu_0 + \frac{c_1(\mu_1-\mu_0)\,\bar{\mu}}{\bar{\mu} + 2S_{1212}(\mu_1-\bar{\mu})} \qquad (4\ a)$$

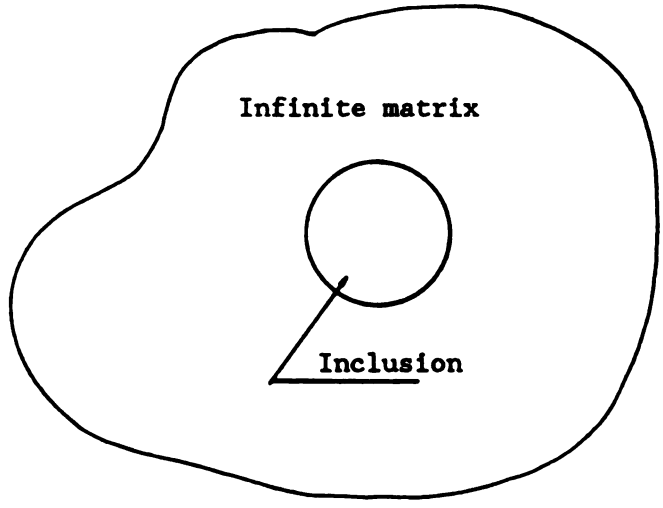

Figure 1.1. Two phase model

(a fiber is embedded in an infinite matrix medium)

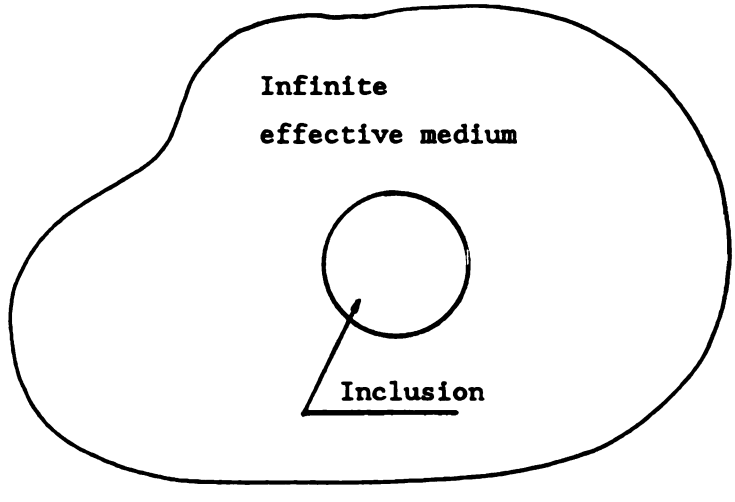

Figure 1.2. Modified two phase model

(a fiber is embedded in an infinite effective medium)

$$\bar{K} = K_0 + \frac{3c_1(K_1-K_0)\,\bar{K}}{3\bar{K} + S_{iijj}(K_1-\bar{K})} . \qquad (4\ b)$$

In the case of a spherical inclusion, $S_{1212} = (4-5\bar{\nu})/15(1-\bar{\nu})$, $S_{iijj} = (1+\bar{\nu})/(1-\bar{\nu})$ and $\bar{\nu} = (3\bar{K} - 2\bar{\mu})/2(\bar{\mu}+3\bar{K})$. The effective moduli $\bar{\mu}$ and $\bar{K}$ can be determined by solving equations (4 a) and (4 b) simultaneously. For inclusions much stiffer than the matrix, equations (4) overestimate the effective moduli while for inclusions much more compliant than the matrix, the effective moduli are underestimated.

More generalized versions of self-consistent methods have been proposed by Hashin [11], 1968, and Christensen and Lo [12], in 1979, for the thermal conduction and elasticity problems respectively. In their generalized versions of self-consistent methods, a model consisting of an inclusion of radius *a* and a concentric matrix shell with radius *b* was embedded in an effective medium as shown Figure 1.3. The generalized self-consistent method appears to be a more realistic approximation than the first version of the method. However the ratio $\eta = a/b$ is an unknown parameter and the choice of η for a spherical inclusion is not obvious.

In early 1960's, Hashin and Shtrikman [13,14,15] obtained improved bounds for the effective elastic moduli of a statistically isotropic composite material on the basis of the energy theorems of classical elasticity. The minimum complementary energy theorem yields the lower bound, while the minimum potential energy theorem yields the

upper bound. In general their method gave better bounds than the Voigt and Reuss bounds and also provided good agreement with experimental data. Hashin and Shtrikman's variational method has been generalized and modified by Hill [16], Walpole [17,18], Wu [19] and others [20,21]. The bounds are of practical value for a fiber/matrix stiffness ratio up to approximately 10. Since the only geometrical information is volume fraction, they can not provide good estimates for extreme stiffness ratios such as a rigid or empty inclusion.

To improve the bounds of the effective moduli, it is necessary to incorporate additional geometrical information. Assuming rectangular packing and perfect bonding between the two constituents, Adams and Doner [22,23], in 1967, examined the effective shear and transverse Young's moduli of composite materials by a finite difference analysis. Because of the assumed periodicity, they were able to isolate a fundamental or repeating element as typical of the entire composite, see Figure 1.4. They formulated the effective moduli in terms of the average elastic stresses and strains obtained by solution of an elasticity boundary-value problem. From their results, Adams and Doner concluded that the predictions of shear and Young's moduli of a square array of fibers is in more reasonable agreement with experimental measurements than those obtained assuming a hexagonal array of fibers.

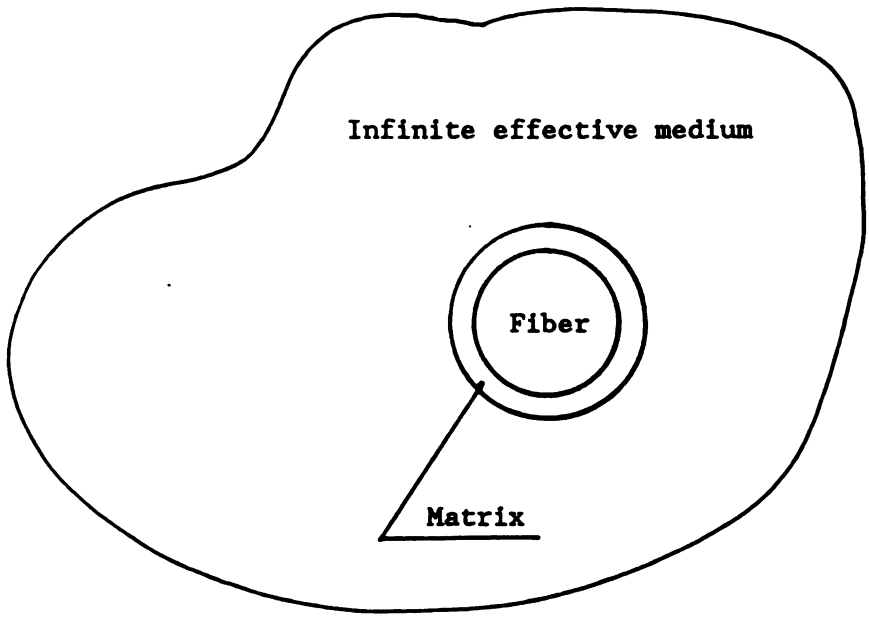

Figure 1.3. Three phase model

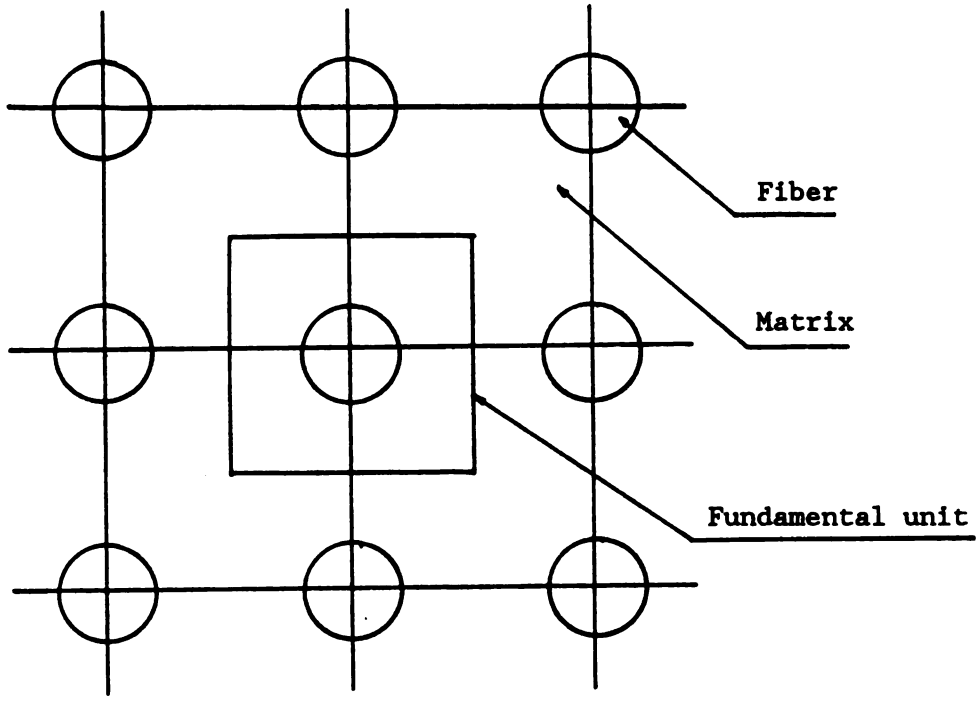

Figure 1.4. Rectangular array model

Chen and Cheng [24] considered a hexagonal array of fibers and defined a triangular fundamental element. They assumed that the fiber and the matrix were homogeneous and isotropic on the microscopic level. Assuming perfect bonding of the interface of the fiber and matrix, they obtained a solution by a combination of the least squares method and the Fourier method. Springer and Tsai [25] approached the effective thermal conductivity problem based on the analogy between the response of the unidirectional composite to shear loading [22] and heat transfer. Without considering thermal contact resistance, they considered a square array and modeled the fundamental element as rectangular. From their results, the transverse effective thermal conductivity was in reasonable agreement with experimental data.

In 1977, similar to Springer and Tsai [25], Gogól and Furmański [26] predicted the transverse thermal conductivity of a rectangular fundamental element by a finite element analysis. From their results, the prediction of the conductivity, κ_{22}, was in good agreement with experimental results except for at high fiber/matrix thermal conductivity ratios ($\kappa_f/\kappa_m > 100$) and high fiber volume fractions. They also concluded that a finite element analysis gave accurate results up to 0.6 percent fiber volume fractions.

The most commonly adopted premise in the theory of the mechanical and thermal behavior of composites is the requirement of continuity of tractions and displacements (in elasticity problems) or temperatures and normal heat flux (in heat transfer problems) at the constituent

interfaces. Such perfect interface conditions, assumed by previous investigators, are a convenient idealization which have given valid results in a large variety of situations [28]. However, internal micro-cracks, voids, debonding and imperfect contact are well known to exist in composite materials. Incorporation of such phenomena in the general theory of effective properties requires the modification and relaxation of the continuity conditions between the constituents. In 1982, Lene and Leguillon [27] examined the equivalent behavior of an elastic composite material when a tangential slip was allowed on the interface of the components. They assumed tangential slip to be a linear law in terms of a scalar coefficient k:

$$\sigma_t\Big|_{S_{12}} = k\left(u_t^{(2)}\Big|_{S_{12}} - u_t^{(1)}\Big|_{S_{12}} \right)$$

where S_{12} is the interface between fiber and matrix and superscripts "1" and "2" indicate that the relevant quantities are associated with the matrix and inclusion respectively. They used an asymptotic expansion method for the unstressed periodic-structure material and employed a finite element analysis. Their results showed the existence of two limit values (D_m and D_M) of a damage coefficient D expressed in terms of k ($D = \log\{(10^4 E_f/k)+1\}$). For $D < D_m$, the material behaved like the perfectly bonded composite. In the intermediate range, the elastic properties of the equivalent material rapidly decreased. For $D > D_M$, a damaged state of the material was reached.

In 1985, Benveniste [28] made the same tangential slip assumptions at the fiber-matrix interface. Based on Christensen and Lo's [12] generalized version of the self-consistent scheme, he

formulated the representative volume average of the elastic strain energy in terms of the surface tractions and displacements using the divergence theorem. From his results, he concluded that the effective shear modulus agreed with Christensen and Lo's predictions when the debonding parameter R ($-1/k$) was zero (perfect bonding) and, as the debonding parameter increased, the effective shear modulus asymptotically decreased.

For periodically distributed inhomogeneities, Mura, Jasiuk, Kouris and Furuhashi [29] examined an extreme case of imperfect bonding of the interfaces. They employed the equivalent inclusion method to evaluate the effect of pure sliding of the interface on the overall elastic constants. They developed an iteration method and obtained an approximation formula for the average shear modulus. From their results, the sliding caused relaxation of the average shear modulus and the relaxation was higher for larger ratios of the inclusion shear and matrix moduli.

In 1988, Jasiuk, Mura and Tsuchida [30] examined the thermal stresses and effective thermal expansion coefficients of a spheroidal fiber composite in which the fiber-matrix interface was allowed to slip. Neglecting the effect of friction, they employed the Boussinesq-Papkovich displacement potential method to solve the stress and displacement disturbances due to a spheroidal inhomogeneity embedded in the matrix. The Mori-Tanaka theorem [31] was used to predict the average thermal expansion coefficients of the composite containing a finite concentration of fibers. From their results, they

observed that sliding at the fiber-matrix interface caused higher stress concentrations and significantly affected the average coefficients of thermal expansion of the composite.

Assuming an initial stress free condition, previous investigators have predicted the effective thermal and mechanical properties by various analytical and numerical schemes. However, high performance fiber composite materials are normally cured at elevated temperature and severe thermally-induced residual stresses may develop in the vicinity of the fibers because of the mismatch of the coefficients of thermal expansion and elastic moduli between the fibers and the surrounding matrix. The presence of residual stresses in fiber composites can not be avoided because the most commonly used method of reducing their intensity (thermal stress relief) can not be applied to such materials. Because of the different thermal expansion characteristics of fiber and matrix, any stresses relieved at the annealing temperature will be re-generated during cooling to ambient temperature [35,37,45].

Some of the detrimental effects caused by such residual stresses are time-dependent dimensional changes, distortion on machining, and reduction of the elastic limit and yield strength of the composites. In a tensile test analysis, the existing state of residual stresses affects the stress-strain response and the performance of the composite [35,37]. For more comprehensive predictions of fiber-reinforced composite material performance, full knowledge of the thermally-induced residual stress distribution is required.

In 1964, Dundurs and Zienkiewicz [32] investigated the stresses in the vicinity of a long circular cylindrical elastic inclusion embedded in an infinite surrounding elastic material subjected to a uniform temperature gradient in a direction transverse to the axis of the cylinder. Their solution was based on an Airy stress function which they obtain by superposition of a "zero-stress" solution and a second solution introduced in order to cancel multivalued and discontinuous displacements arising in the first solution. The problem could be solved in a direct way using the thermal potential function derived by Sternberg and McDowell [33] and Tauchert [34].

Instead of an infinite matrix with a single embedded fiber, Hecker, Hamilton and Ebert [35] examined a concentric cylindrical OFHC copper-4340 steel composite in 1969. They developed a modified Sachs [36] boring-out procedure to obtain an experimental measure of the intensity and distribution of residual stresses due to cool-down from final heating temperature. From their semi-empirical results, they concluded that the magnitudes of the residual stresses in the fabricated composite were very high, e.g. in the copper core region, they greatly exceeded the yield strength in uniaxial tension. In a later paper [37], they formulated an elastic solution to predict thermally-induced residual stresses for their previous concentric cylindrical composites. They assumed that the interfacial bond was perfect and the residual stresses resulted only from the difference in thermal expansion coefficients between homogeneous, isotropic elastic components. From their results, they concluded that the theoretical

predictions and the experimental results of residual stresses differed by less than 25 percent.

During fabrication of metal matrix composites, thermally-induced local plastic deformation can occur. To account for these plastic strains Hoffman [38], in 1973, estimated the magnitude of elastic stresses and elastic-plastic stresses and strains in a tungsten fiber-reinforced 80 Ni+20 Cr matrix composite during heating and cooling between 80 and 2000 deg F. He developed approximate equations for high fiber volume and low fiber volume fractions of fibers in homogeneous, isotropic components. A hydrostatic stress state within each constituent had been assumed in the high volume fraction of fibers. However, in the low volume fraction of fibers, he used thick wall cylinder theory in the derivation and included the possibility of plastic strains. In his derivation, he did not consider either a metallurgical interphase or stresses due to differences in the Poisson's ratios of fiber and matrix. He concluded that large elastic stresses, sufficient to cause fracturing of either constituent or the interface, could quickly occur in cyclic temperature usage.

In 1978, Miller and Adams [39] approached a more realistic behavior of composites. They modeled a micro-region, consisting of a square matrix containing a cylindrical fiber, by means of the finite element method. They assumed inelastic matrix behavior, an elastic fiber and a state of generalized plane strain. They calculated stresses due to cool down from curing temperature and moisture absorption in graphite/epoxy composites. The results indicated that,

for 60 percent fiber volume fraction, the maximum residual stresses were on the order of the yield strength of the matrix material.

In 1979, Uemura, Iyama and Yamaguchi [40], assuming the matrix to be isotropic and the cylindrical fibers to be transversely isotropic in carbon reinforced composites, calculated thermally-induced residual stresses using effective thermal expansion coefficients and effective mechanical properties. Experiments on carbon-fiber/epoxy composite cylinders showed good agreement with the theoretically predicted values. They concluded that the residual stresses induced by curing could not be neglected when compared with the low tensile strength transverse to the fibers.

In 1979, Weitsman [41] and Herrmann and Mattheck [42], rather than applying linear thermo-elastic theory, proposed a visco-elastic response of the matrix and accounted for temperature-dependence and stress sensitivity of the creep compliance. Comparisons with linear elastic solutions indicated that the viscoelastic relaxation may reduce the residual stresses by about 20 percent.

In 1986, Rohwer and Jiu [43] studied the effects of free edge conditions during the curing process. They employed a three dimensional finite element model for calculation of residual stresses in a hexagonal array of fibers. Concentrations of radial and tangential stresses were found along the free edge interface. The matrix was predominantly endangered by high tangential and axial stresses arising at a certain distance from the free edge.

In 1986, Avery and Herakovich [44] utilized an elastic solution to analyze orthotropic fibers in an isotropic matrix. They showed that, for orthotropic fibers, stress distributions are radically different than those predicted assuming the fiber to be transversely isotropic. Fiber volume fraction greatly influences the stress distribution for transversely isotropic fibers, but has little effect on the distribution if the fibers are transversely orthotropic.

In 1987, Adams [45] studied the influence of interface degradation, and thermal and moisture effects on the performance of various carbon fiber-reinforced unidirectional composite materials. For a square packing array of circular fibers, he calculated hygrothermal stresses using a two dimensional finite element model. The predicted thermal residual normal stress at the fiber-matrix interface for 0.6 volume fiber fraction of ASA/3501-6 was compressive, the highest values occurring in the regions of closest fiber spacing. At 16 MPa, it was approximately 25 percent of the tensile strength of the Hercules 3501-6 epoxy matrix. The addition of 2.9 weight percent moisture to the matrix induced residual stresses of magnitudes over 2.3 times those induced during cool down.

In 1988, Vedula, Pangborn, and Queeney [46] examined the effect of anisotropy of the fiber thermal expansion properties by extending a thick-walled cylinder model that had been developed for a graphite/aluminum composite in which the fiber and matrix materials had isotropic elastic moduli. They showed that transverse thermal

stresses are 75 percent lower for the case of anisotropic thermal expansion coefficients than for the isotropic case. They also showed that, when these stresses were examined for incipient plasticity, anisotropy of the fiber thermal expansion can result in a large temperature range of elastic deformation during cooling from processing temperatures. In a later paper [47], they examined a three-component cylinder model of a unidirectional composites. The components consisted of the fiber, an interfacial coating region and a surrounding matrix. As in their previous paper, they assumed that all three components had homogeneous and isotropic elastic mechanical properties and the fiber had anisotropic thermal expansion coefficients. Under the assumption of perfect bonding of the three components, they concluded that the existence of the interfacial region contributed significantly to residual stress build-up. Furthermore, the use of a third coating component in the form of an interfacial region could control the intensity of the residual thermal stresses.

Finally, Hahn and Kim [48], instead of an interfacial region model, proposed that the concentric fiber and matrix were surrounded by an infinite homogeneous medium that had the properties of the composite, as in Figure 1.3. They assumed that the interfacial bonds were perfect, the fiber and the composite were homogeneous and transversely isotropic and the matrix was isotropic. Their three-phase model predicted a compressive radial stress of 1.1 MPa at room temperature (25 ^{o}C) after cool-down from 60 ^{o}C cure temperature along the fiber/matrix interface of a Kevlar 49/epoxy composite. They also

performed a finite element analysis for a square array of fibers. The results indicated that the maximum compressive radial stress was in the region of closest fiber spacing. From their three-phase model and finite element analysis results, they concluded that the predicted radial stress, by the three-phase model, was comparable to the average stress over the fiber surface determined by the finite element analysis.

A number of investigators [49,50] have discussed the presence of a thin interphase region between fiber and matrix, of different material properties. Others [51,52,53] have discussed the existence of voids and micro-cracks in the interface and the possibility of imperfect bonding. Voids, formed during fabrication, and cracks, formed due to differential thermal contraction, significantly reduce the elastic moduli from the expected values [54].

The primary motivation of the present work is to develop techniques for better understanding how various types of interface conditions and thermally-induced residual stresses can influence the thermal and mechanical behavior of the composite material. Past investigations have been aimed primarily at evaluation of the effective elastic constants in composites with perfect bonding of the interface and results have been obtained in closed-form or by finite element analysis.

In Chapter 2, the boundary element method is formulated for the plane strain thermo-elasticity problem. In the Navier's equations,

written in terms of displacement, thermal load is treated as an effective body force. As is usual in boundary element analysis, the body force is treated using a domain integration. However, in this formulation, the domain integration can be transformed to a boundary integration by defining the Galerkin tensor and employing the divergence theorem.

In Chapter 3, two fundamentally important concepts are introduced for the calculation of thermally-induced residual stresses during the cool-down process. First, we assume the composite medium to be macroscopically homogeneous and isotropic or transversely isotropic. Instead of considering the entire composite medium, we isolate a single fiber and it's surrounding matrix region as a fundamental unit cell which represents behavior of the entire composite. Second, the macroscopically-homogeneous medium will be deformed uniformly during the cool-down process. Since the deformation of a fundamental unit must be consistent with the entire medium, we use the superposition technique with displacement-controlled boundary conditions.

In Chapter 4, in order to estimate effective elastic properties of the composite material, we examine the "balance of work and energy" theorem. Due to lack of a proper technique for prediction of crack development due to thermal residual stresses and phases of differing elastic properties, we introduce two different damage material models. These are the interphase degradation model and the tangential displacement discontinuity model. For each of these damaged models, we

will examine the elastic moduli of the damaged material.

Finally, in Chapters 5 and 6, we will apply and discuss our boundary element technique to obtain results for thermally-induced residual stresses and effective elastic behavior of fiber-reinforced composites assuming both a perfect bond interface and a damaged interface. We will also examine our present method in comparison with other published results.

CHAPTER 2

BOUNDARY ELEMENT METHOD

2.1 Governing equations for thermoelasticity problems

Plane strain thermoelasticity problems are considered in this analysis. The cross-section of the composite body is assumed to lie in the x_2-x_3 plane, which is perpendicular to the fiber direction x_1 as shown in Figure 2.1. The first assumption made for this problem is that each component of the strain tensor ϵ_{ij} can be additively decomposed into elastic and thermal parts, $\epsilon_{ij}^{(e)}$ and $\epsilon_{ij}^{(T)}$, respectively. Thus,

$$\epsilon_{ij} = \epsilon_{ij}^{(e)} + \epsilon_{ij}^{(T)} = \epsilon_{ij}^{(e)} + \alpha T \delta_{ij} \tag{2.1}$$

where α is the coefficient of thermal expansion, T is the change in temperature and δ_{ij} is the Kronecker delta. The range of indices in equation (2.1) is i=2,3 ; j=2,3. The equations of equilibrium can be written in terms of displacements by combining them with the constitutive and kinematic equations. The governing equation, expressed in terms of displacements, for an elastic homogeneous isotropic medium under thermal loading is :

$$G\, u_{i,jj} + \frac{G}{1-2\nu}\, u_{k,ki} = -F_i + 2G \left(\frac{1+\nu}{1-2\nu} \right) \alpha\, T_{,i} \tag{2.2}$$

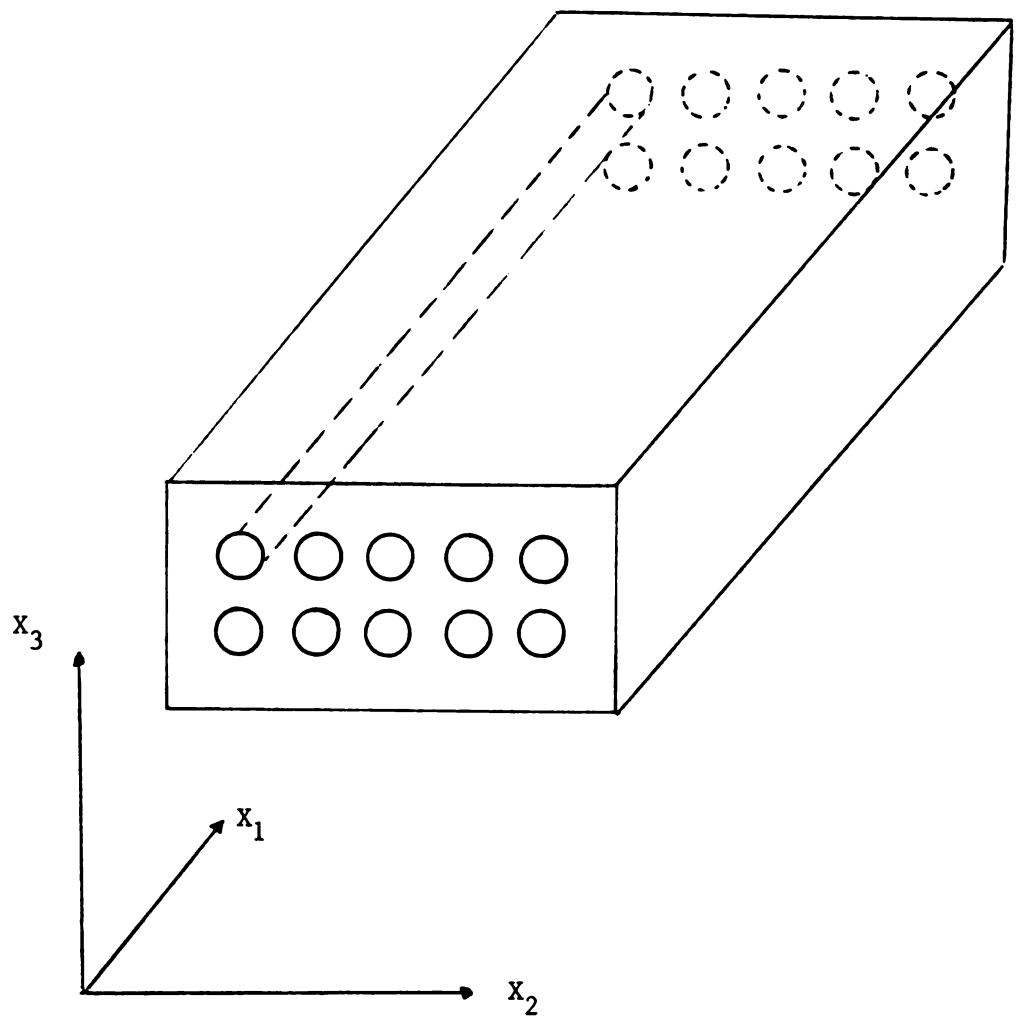

Figure 2.1 Unidirectional fiber-reinforced composite

where G is the shear modulus, ν is Poisson's ratio and F_i are the components of the body force vector per unit volume. The partial differential equations (2.2) must be solved subject to the appropriate boundary conditions. The usual mechanical boundary condition, i.e. displacement, traction, or combination, must be prescribed on the boundary Γ of the body. The components of the traction vector t_i at a point on the boundary Γ are given by

$$t_i = G\left[\left((u_{i,j} + u_{j,i})n_j + \frac{2\nu}{1-2\nu}\, u_{k,k}\, n_j\right) - \frac{2(1+\nu)}{1-2\nu}\, \alpha T n_i\right] \qquad (2.3)$$

where n_i are the components of the unit outward normal to Γ at that point.

2.2 Direct BEM formulation for displacement

A boundary element method (BEM) formulation for the displacement field is obtained by following the method outlined by Danson [55]. Kelvin's fundamental solution, chosen here as the auxiliary solution, is [56] :

$$u_i^* = U_{ij}\, e_j \qquad (2.4)$$

where u_i^* satisfies the equation

$$u^*_{i,jj} + \frac{1}{1-2\nu}\, u^*_{k,ki} = -\frac{\Delta(\Phi,\Xi)}{G}\, \delta_{ij}\, e_j. \qquad (2.5)$$

In equation (2.5), Δ is the Dirac delta function and e_j are unit orthogonal base vectors. The two point influence function U_{ij} is the displacement in the i direction at a field point Φ due to a unit load

in the j direction at a source point Ξ. The function U_{ij} for plane strain is available in many references [55,56,57,58,59]. The traction vectors t_i^* in the homogeneous elasticity problem are related to the gradients of the displacement field according to the equation

$$t_i^* = G \left[(u_{i,j}^* + u_{i,j}^*)\, n_j + \frac{2\nu}{1-2\nu}\, u_{k,k}^*\, n_i \right]. \tag{2.6}$$

Multiplying both sides of equation (2.2) by u_i^* and integrating over the domain Ω of the body results in the equation

$$\int_\Omega u_i^* \left[G\, u_{i,jj} + \frac{G}{1-2\nu}\, u_{k,ki} \right] d\Omega$$

$$- \int_\Omega u_i^* \left[-F_i + 2G\, \frac{1+\nu}{1-2\nu}\, \alpha\, T_{,i} \right] d\Omega \,. \tag{2.7}$$

Using the definitions of tractions from equations (2.3), (2.6), and the divergence theorem, equation (2.7) can be reduced to

$$u_i(\Phi) + \int_\Gamma T_{ij}(\Phi,\bar{x})\, u_i(\bar{x})\, d\Gamma_{\bar{x}} - \int_\Gamma U_{ij}(\Phi,\bar{x})\, t_i(\bar{x})\, d\Gamma_{\bar{x}}$$

$$+ \int_\Omega U_{ij,j}(\Phi,\Xi) \left[\frac{E}{1-2\nu}\, \alpha\, T\,(\Xi) \right] d\Omega_\Xi$$

$$- \int_\Omega U_{ij}(\Phi,\Xi)\, F_i(\Xi)\, d\Omega_\Xi \tag{2.8}$$

where the two point influence function $T_{ij}(\Phi,\bar{x})$ is the traction in the i direction at a field point Φ due to a unit load in the j direction at

a source point $\bar{x}$, Φ and Ξ denote points inside the body Ω and x and $\bar{x}$ denote points on the boundary Γ. Equation (2.8) is seen to contain the unknown temperature field inside both the domain integrals and the boundary integrals. The temperature field must be obtained by solving the diffusion equation with the appropriate thermal boundary conditions. The domain integrals which contain the body force $F_i(\Xi)$ and thermal loads (effective body force) must be dealt with by dividing the domain Ω into integration cells, thus increasing the amount of data preparation required to run a particular problem, e.g. plasticity problems [60], viscoelasticity problems [61] or nonhomogeneous problems [62]. However Cruse [56] and Danson [55] have shown that for many of the commonly-encountered body forces such as gravity, rotational inertia or steady state thermal loads, the domain integrals in equation (2.8) may be reduced to a surface integral by a further application of the divergence theorem. In this analysis, the thermal load is considered to be the only non-zero domain integral.

2.3 Transformation of domain integrals to boundary integrals

Let's denote the domain integral in equation (2.8) as an effective body force vector $B_i(\Phi)$

$$B_i(\Phi) = \int_\Omega U_{ij,j}(\Phi,\Xi) \left[\frac{E}{1-2\nu} \alpha T(\Xi) \right] d\Omega_\Xi . \qquad (2.9)$$

In order to transform the domain integral, equation (2.9), to an equivalent boundary integral, it is useful to define a tensor $G_{ij}(\Phi,\Xi)$ (the Galerkin tensor) such that the displacement kernel $U_{ij}(\Phi,\Xi)$ is

given by

$$U_{ij}(\Phi,\Xi) = G_{ij,kk}(\Phi,\Xi) - \frac{G_{ij,kj}(\Phi,\Xi)}{2(1-\nu)} \quad . \tag{2.10}$$

Differentiating the Galerkin tensor $G_{ij}(\Phi,\Xi)$ and renaming dummy indices gives

$$U_{ij,j}(\Phi,\Xi) = \frac{1-2\nu}{2(1-\nu)} G_{ij,jkk}(\Phi,\Xi). \tag{2.11}$$

Thus, the domain integral $B_i(\Phi)$ becomes

$$B_i(\Phi) = \int_\Omega U_{ij,j}(\Phi,\Xi) \left[\frac{E}{1-2\nu} \alpha T(\Xi)\right] d\Omega_\Xi$$

$$- \int_\Omega G_{ij,jkk}(\Phi,\Xi) \left[\frac{E}{1-2\nu}\alpha T(\Xi)\right] d\Omega_\Xi. \tag{2.12}$$

For steady state heat conduction $T_{,jj}(\Xi)=0$ and one may write

$$B_i(\Phi) = \frac{\alpha E}{1-2\nu} \int_\Omega \left(G_{ij,jkk}(\Phi,\Xi)\, T(\Xi) - G_{ij,j}(\Phi,\Xi)\, T_{,jj}(\Xi)\right) d\Omega_\Xi.$$

(2.13)

Using the divergence theorem, equation (2.13) can be transformed to a boundary integral as :

$$B_i(\Phi) = \frac{\alpha E}{1-2\nu} \int_\Gamma \left(G_{ij,jk}\ (\Phi,\bar{x})\ T(\bar{x}) - G_{ij,j}(\Phi,\bar{x})\ T_{,k}(\bar{x})\right) n_k d\Gamma_{\bar{x}}.$$

(2.14)

The boundary integral expression for displacements for the

thermoelasticity equation (2.8) may now be obtained by taking the limit as an internal point Φ approaches a point $\mathbf{x}$ on boundary Γ

$$c_{ij}(\mathbf{x})\, u_j(\mathbf{x}) + \int_\Gamma T_{ij}(\mathbf{x},\bar{\mathbf{x}})\, u_i(\bar{\mathbf{x}})\, d\Gamma_{\bar{\mathbf{x}}} = \int_\Gamma U_{ij}(\mathbf{x},\bar{\mathbf{x}})\, t_i(\bar{\mathbf{x}})\, d\Gamma_{\bar{\mathbf{x}}}$$

$$+ \int_\Gamma P_i(\mathbf{x},\bar{\mathbf{x}})\, T(\bar{\mathbf{x}})\, d\Gamma_{\bar{\mathbf{x}}} - \int_\Gamma Q_i(\mathbf{x},\bar{\mathbf{x}})\, T_{,k}(\bar{\mathbf{x}})\, n_k\, d\Gamma_{\bar{\mathbf{x}}} \qquad (2.15)$$

where

$$U_{ij}(\mathbf{x},\bar{\mathbf{x}}) = \frac{(1+\nu)}{4\pi E(1-\nu)} \left[\left\{ (3-4\nu)\ln\left(\frac{1}{r}\right) - \frac{7-8\nu}{2} \right\} \delta_{ij} + r_i r_j \right]$$

$$T_{ij}(\mathbf{x},\bar{\mathbf{x}}) = \frac{(1+\nu)}{4\pi(1-\nu)r} \left[n_k r_k \{(1-2\nu)\delta_{ij} + 2r_i r_j\} - (1-2\nu)(r_i n_j - r_j n_i) \right]$$

$$G_{ij}(\mathbf{x},\bar{\mathbf{x}}) = \frac{1+\nu}{4\pi E}\, \delta_{ij}\, r^2 \ln\left(\frac{1}{r}\right)$$

$$P_i(\mathbf{x},\bar{\mathbf{x}}) = \frac{\alpha(1+\nu)}{4\pi(1-\nu)} \left\{ \left(\ln\left(\frac{1}{r}\right) - \frac{1}{2} \right) n_i - n_k r_k r_i \right\}$$

$$Q_i(\mathbf{x},\bar{\mathbf{x}}) = \frac{\alpha(1+\nu)}{4\pi(1-\nu)}\, r_i r \left(\ln\left(\frac{1}{r}\right) - \frac{1}{2} \right). \qquad (2.16)$$

and

$$r^2 = \left[(x_1 - \bar{x}_1)^2 + (x_2 - \bar{x}_2)^2 \right]$$
$$r_i = (x_i - \bar{x}_i)/r \,. \qquad (2.17)$$

The tensor $c_{ij}(\mathbf{x})$ is a function of the local geometry and the location of $\mathbf{x}$. If the boundary is locally smooth at $\mathbf{x}$, $c_{ij}(\mathbf{x}) = \frac{1}{2}\, \delta_{ij}$. As

shall be seen, knowledge of $c_{ij}(x)$ is not required.

Once the displacement and traction fields have been obtained everywhere on the boundary using equations (2.15), the displacements and stresses for any internal point Φ of the body can be calculated from the equations

$$u_i(\Phi) = \int_\Gamma U_{ij}(\Phi,\bar{x})\ t_j(\bar{x})\ d\Gamma_{\bar{x}} - \int_\Gamma T_{ij}(\Phi,\bar{x})\ u_j(\bar{x})\ d\Gamma_{\bar{x}}$$

$$+ \int_\Gamma P_i(\Phi,\bar{x})\ T(\bar{x})\ d\Gamma_{\bar{x}} - \int_\Gamma Q_i(\Phi,\bar{x})\ T_{,k}(\bar{x})\ n_k\ d\Gamma_{\bar{x}}$$

$$\sigma_{ij}(\Phi) = \int_\Gamma D_{kij}(\Phi,\bar{x})\ t_k(\bar{x})\ d\Gamma_{\bar{x}} - \int_\Gamma S_{kij}(\Phi,\bar{x})\ u_k(\bar{x})\ d\Gamma_{\bar{x}}$$

$$+ \int_\Gamma S^*_{ij}(\Phi,\bar{x})\ T(\bar{x})\ d\Gamma_{\bar{x}} - \int_\Gamma V^*_{ij}(\Phi,\bar{x})\ T_{,k}(\bar{x})\ n_k\ d\Gamma_{\bar{x}} - \frac{\alpha E}{1-2\nu}\ T(\bar{x})\delta_{ij}. \tag{2.18}$$

where the influence functions D_{kij}, S_{kij}, S^*_{ij} and V^*_{ij} are derived from the displacement gradient and stress-displacement relations.

2.4 Numerical implementation of BEM

The boundary of the body Γ is discretized into N straight segments, as shown in Figure 2.2. A discretized version of equation (2.15) is written as

$$c_{ij}^{(n)}(\mathbf{x})\, u_j^{(n)}(\mathbf{x}) + \sum_{m=1}^{N} \int_{\Gamma_m} T_{ij}(\mathbf{x},\bar{\mathbf{x}})\, u_j(\bar{\mathbf{x}})\, d\Gamma_{\bar{\mathbf{x}}_m}$$

$$- \sum_{m=1}^{N} \int_{\Gamma_m} U_{ij}(\mathbf{x},\bar{\mathbf{x}})\, t_j(\bar{\mathbf{x}})\, d\Gamma_{\bar{\mathbf{x}}_m} + \sum_{m=1}^{N} \int_{\Gamma_m} P_i(\mathbf{x},\bar{\mathbf{x}})\, T(\bar{\mathbf{x}})\, d\Gamma_{\bar{\mathbf{x}}_m}$$

$$- \sum_{m=1}^{N} \int_{\Gamma_m} Q_i(\mathbf{x},\bar{\mathbf{x}})\, T_{,k}(\bar{\mathbf{x}})\, n_k\, d\Gamma_{\bar{\mathbf{x}}_m} . \qquad (2.19)$$

where $u_j(\mathbf{x})^{(n)}$ are the displacements components at node n and n=1,2,.....,N, j=2,3.

After having determined the temperature and heat flux distributions on the boundary Γ, suitable shape functions must be chosen to represent the displacement, traction, temperature and heat flux on Γ. Displacement components are assumed to be piecewise linear on the boundary segments Γ_m. However, the traction components and temperature and heat flux are assumed to be constant on the boundary segments, i.e.

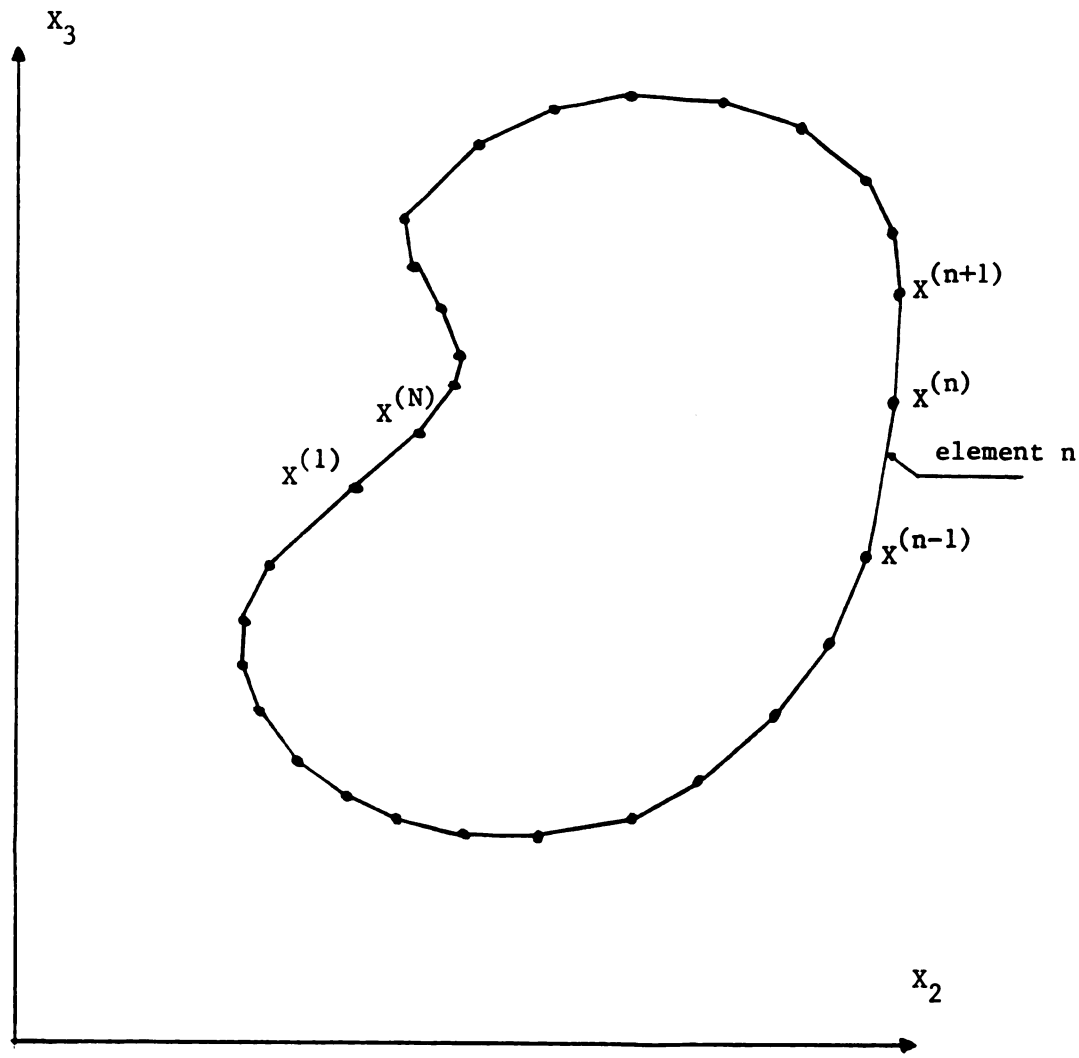

Figure 2.2. Discretized boundary element

$$u_j(\bar{x}) = u_j^{(m-1)} N_1(\xi) + u_j^{(m)} N_2(\xi)$$

$$t_j(\bar{x}) = t_j^{(m)}$$

$$T(\bar{x}) = T^{(m)}$$

$$T_{,n}(\bar{x}) = T_{,n}^{(m)} \tag{2.20}$$

where

$$N_1(\xi) = (1-\xi)/2,\ N_2(\xi) = (1+\xi)/2$$

$$\bar{x} = N_1(\xi)\, x^{(m-1)} + N_2(\xi)\, x^{(m)}$$

$$d\Gamma_m = \left[\frac{1}{2}(s_m - s_{m-1})\right] d\xi = (\Delta s_m/2)\, d\xi \tag{2.21}$$

and ξ is a local coordinate for the segment m with value -1 at node m-1, value 0 at the center of the segment, and value 1 at node m.

Note that the order of traction $t_j(x)$ in the interval is less than that of displacement $u_j(x)$ on the boundary and it is consistent within elements, i.e. linear displacements and constant tractions on each element. If equations (2.18) and (2.19) are substituted into equations (2.17) the following is obtained

$$2c_{ij}^{(n)}(x)\, u_j^{(n)}(x) + \Delta s_m \sum_{\substack{m=1 \\ m \neq n+1}}^{N} \int_{\Gamma_m} T_{ij}(x,\xi)\, N_1(\xi)\, d\xi \cdot u_j^{(m-1)}$$

$$+ \Delta s_m \sum_{\substack{m=1 \\ m \neq n}}^{N} \int_{\Gamma_m} T_{ij}(x,\xi)\, N_1(\xi)\, d\xi \cdot u_j^{(m)} = \Delta s_m \sum_{m=1}^{N} \int_{\Gamma_m} U_{ij}(x,\xi)\, d\xi \cdot t_j^{(m)}$$

$$+ \Delta s_m \sum_{m=1}^{N} \int_{\Gamma_m} P_i(x,\xi)\, d\xi \cdot T^{(m)} - \Delta s_m \sum_{m=1}^{N} \int_{\Gamma_m} Q_i(x,\xi)\, d\xi \cdot T^{(m)}_{,k}\, n^{(m)}_k \,.$$

$$m=1,2,\ldots\ldots,N \qquad (2.22)$$

Equation (2.20) can also be written in matrix form as

$$[\,U\,]\cdot(\,u\,) = [\,T\,]\cdot(\,\hat{t}\,) + (\,b\,) \qquad (2.23)$$

where [U] and [T] are coefficient matrices which can be calculated from the fundamental solutions (2.16). In equation (2.23) the column vectors (u) and ($\hat{t}$) denote the nodal displacement and resultant segment force vectors, respectively, and (b) the column vector corresponding to the resultant segment temperature and heat flux distributions on the boundary. For more detail of the numerical derivations, see reference [63].

CHAPTER 3

THERMAL RESIDUAL STRESSES DUE TO THE CURING PROCESS

3.1 Micro-mechanics of composite materials

To treat the problem analytically, assumptions must be made regarding the fiber packing arrangement and the geometry of the individual fibers. Here, a rectangular fiber packing array has been assumed, as shown in Figure 1.4. A rectangular array, which permits the variation of fiber spacing in two coordinate directions independently, offers more versatility than a hexagonal array which has only one geometry spacing variable. The individual fiber cross-sections are assumed to be symmetrical about each of the coordinate axes, x_2 and x_3. Within this assumption, the fiber can be of arbitrary shape, i.e., circular, elliptical, diamond, square, rectangular, hexagonal, etc. Because of assumed periodicity, a fundamental or repeating unit, as indicated by the dashed lines of Figure 1.4, can be isolated and considered as typical of the entire composite. Because of the assumed fiber symmetry, only one quadrant of this fundamental unit need be considered.

3.2 Stress analysis

Having established the fundamental unit by assuming rectangular

packing and doubly symmetric cylindrical fibers, the problem can be formulated exactly by the theory of thermo-elasticity. Let u_i denote the components of the displacement vector field. Then the components of the infinitesimal strain field are

$$\epsilon_{ij} = \frac{1}{2} (u_{i,j} + u_{j,i}). \tag{3.1}$$

The constitutive equations for a homogeneous elastic medium are

$$\sigma_{ij} = C_{ijkl} \epsilon_{kl} - \beta_{ij} T \tag{3.2}$$

where C_{ijkl} and β_{ij} are constitutive coefficients that obey certain symmetry relations, e.g. $C_{ijkl} = C_{ijlk}$. Thus constitutive equation (3.2) can be expressed in terms of displacement as

$$\sigma_{ij} = C_{ijkl} u_{k,l} - \beta_{ij} T. \tag{3.3}$$

We assume the matrix to be isotropic and homogeneous and the cylindrical fibers to be transversely isotropic and homogeneous. The change of temperature T is assumed to be uniform throughout the fiber-reinforced composite material. Assuming a state of isothermal generalized plane strain for the fundamental unit, equation (3.3) can be written as

$$\sigma_{ij} = \frac{\nu E \delta_{ij}}{(1-\nu)(1-2\nu)} u_{k,k} + \frac{E(u_{i,j}+u_{j,i})}{2(1+\nu)} - \frac{\alpha E T}{(1-2\nu)} \delta_{ij} \tag{3.4}$$

where α is the coefficient of thermal expansion. The equations of equilibrium, in the absence of body force, are

$$\sigma_{ij,j} = 0. \tag{3.5}$$

3.3 Boundary conditions

When the fiber-reinforced composite is subjected to a uniform decrease in temperature, the fibers will move toward each other. At the rectangular boundary during shrinkage, the plane containing $\overline{BC}$, $\overline{CD}$ and parallel to the x_1 axis (fiber axis) remain plane because they are shared by the adjacent rectangular elements (see Figure 1.4) [64]. Therefore, the shear stresses must vanish on the rectangular boundary so that

$$\sigma_{23} = \sigma_{32} = 0. \tag{3.6}$$

Let's first assume the fibers to be fixed in space. In this state, a normal stress $\sigma_{ij}(x_2,x_3)\big|_{fixed}$ is set up along lines $\overline{BC}$ and $\overline{CD}$, while the shear stress equals zero due to symmetry. The system is then released and the fibers permitted to move toward each other. Points B, C and D will move to B′, C′ and D′, respectively. Because of symmetry, lines $\overline{B'C'}$ and $\overline{C'D'}$ will remain straight lines, parallel to $\overline{BC}$ and $\overline{CD}$, respectively. A stress field $\sigma_{ij}(x_2,x_3)\big|_{relaxation}$ is induced by the relaxation of system whose intensity is directly proportional to the normal displacement, as shown in Figure 3.1. Thus

$$\overline{BB'} = \overline{DD'} = u^0. \tag{3.7}$$

Specifying the normal displacement at the boundary, however, has introduced another unknown u^0. The unknown u^0 is indirectly governed by the equilibrium condition for residual stresses in the absence of external loads, i.e., by the fact that sums of normal stresses on the

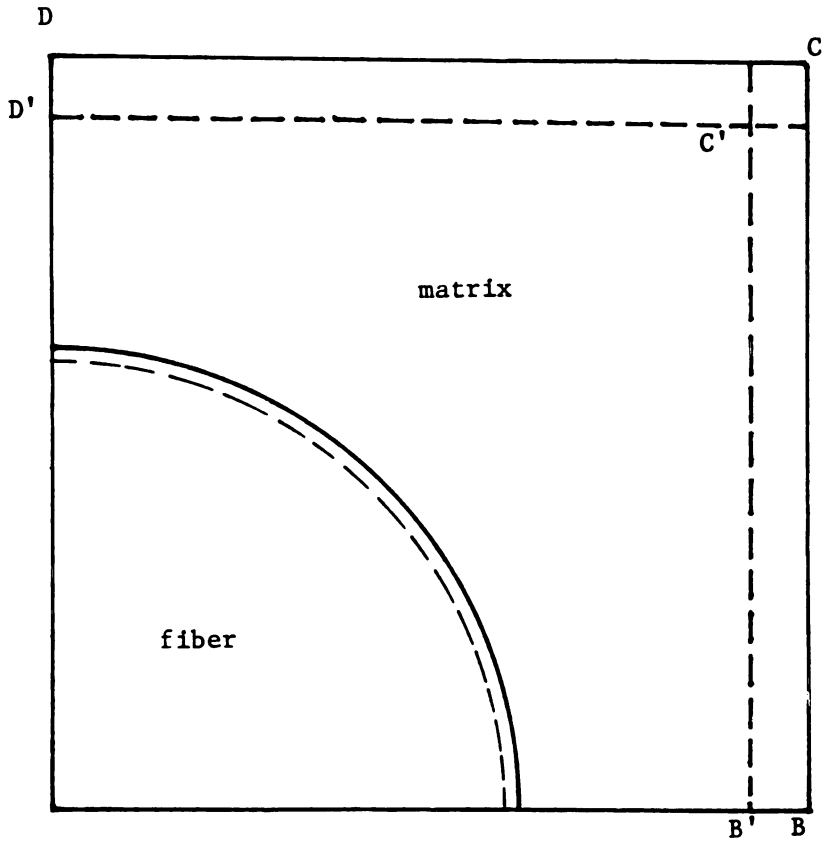

Figure 3.1. Geometry of Shrinkage

lines $\overline{BC}$ and $\overline{CD}$ must be zero. The normal stresses must satisfy the equations

$$\int_B^C \sigma_{22}\, d\Gamma_{BC} = \int_B^C \left[\sigma_{22}|_{fixed} + \sigma_{22}|_{relaxation}\right] d\Gamma_{BC} = 0$$

$$\int_C^D \sigma_{33}\, d\Gamma_{CD} = \int_C^D \left[\sigma_{33}|_{fixed} + \sigma_{33}|_{relaxation}\right] d\Gamma_{CD} = 0. \qquad (3.8)$$

The final residual stress due to cool-down at each point is then

$$\sigma_{ij}|_{residual} = \sigma_{ij}|_{fixed} + \sigma_{ij}|_{relaxation}. \qquad (3.9)$$

The problem is to find the residual stress $\sigma_{ij}|_{residual}(x_2, x_3)$ due to cool-down from the curing temperature. This will be examined by employing a thermoelasticity boundary element analysis.

3.4 B.E.M. applied to a non-homogeneous region

Equations (2.23) are valid for a homogeneous body. Bodies with different material properties can be analyzed by dividing the domain into homogeneous subregions. Consider the fundamental unit of the fiber-reinforced composite, shown in Figure 3.2 (a), formed by the subregions Ω_{fiber} and Ω_{matrix}. We begin by assuming that each subregion "i" is an independent domain and apply equations (2.23) to each, i.e.

$$[\mathbb{U}]^i \cdot (u)^i = [\mathbb{T}]^i \cdot (\hat{t})^i + (b)^i \qquad (3.10)$$

where the summation notation is not implied and $i = 1, 2$. By applying

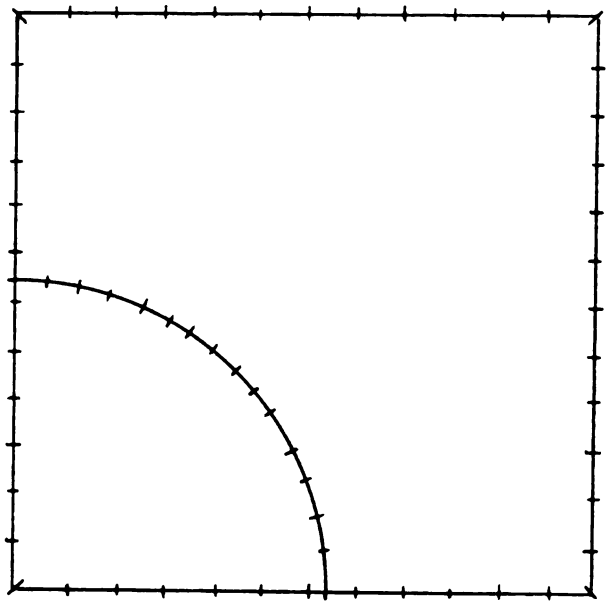

(a) BEM model

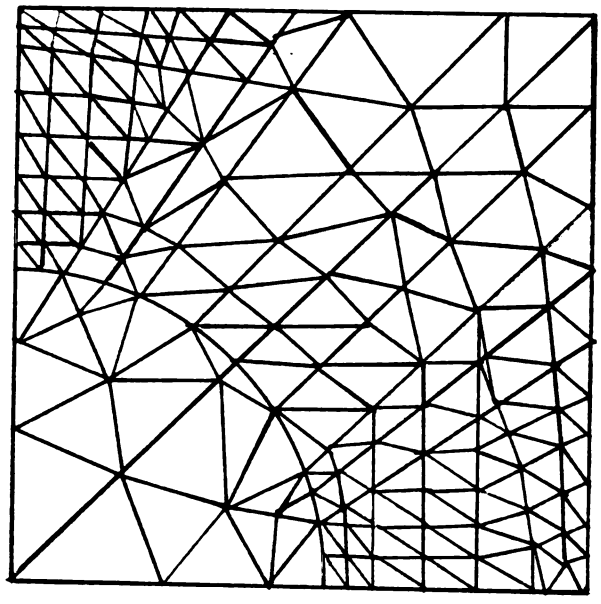

(b) FEM model

Figure 3.2. Typical (a) boundary element segment and (b) finite element grid (Adams ref. 71)

the conditions at the interface Γ_{ij} (common to subregion "*i*" and "*j*"), a global system of equations will be established.

3.5 Interface conditions

Interface conditions result from the assumption that the boundary displacement and traction vectors of the reinforcement fiber and the matrix, $u_i^{(f)}$, $t_i^{(f)}$ and $u_i^{(m)}$, $t_i^{(m)}$ respectively, are connected by analytical relations. During the cool-down process, we assume that two neighboring particles of the two materials remain together during all displacements at the fiber/matrix interface (perfect interface bond).

$$u_i^{(f)} = u_i^{(m)} \qquad \text{on } \Gamma_{interface} \qquad (3.11)$$

In addition, traction equilibrium is given by

$$t_i^{(f)} + t_i^{(m)} = 0. \qquad \text{on } \Gamma_{interface} \qquad (3.12)$$

Chapter 4

THE EFFECTIVE MECHANICAL BEHAVIOR

4.1 Balance of work and energy

Consider the two geometrically identical fundamental units which represent the heterogeneous fiber/matrix composite and the macroscopically homogeneous composite, respectively, as shown in Figure 4.1. Let V_f and V_m denote the volumes of the fiber and matrix respectively and let the interface be denoted by Γ_{fm}. Let V be the volume of the effective composite medium. The external boundary of each medium is denoted by Γ. We assume that the fiber/matrix composite and the effective medium are statistically homogeneous with the effective moduli C^*_{ijkl}, matrix moduli $C^{(m)}_{ijkl}$ and fiber moduli $C^{(f)}_{ijkl}$.

The starting point for examination of the effective moduli C^*_{ijkl} is the "balance of work and energy" theorem for a composite medium [28]. Consider the two unrelated displacements fields u_i and u^*_i and tractions $t_i(\Gamma)$ and $t^*_i(\Gamma)$. u_i, t_i are the displacements and tractions associated with the fiber/matrix medium and u^*_i, t^*_i are those associated with the effective medium. Under the imposed boundary displacement conditions, $u^*_i(\Gamma)$, the external work done on the effective medium is

$$W^* = \frac{1}{2}\int_\Gamma u^*_i\, t^*_i\, d\Gamma = \frac{1}{2}\int_V \sigma^*_{ij}\, \epsilon^*_{ij}\, dV. \qquad (4.1)$$

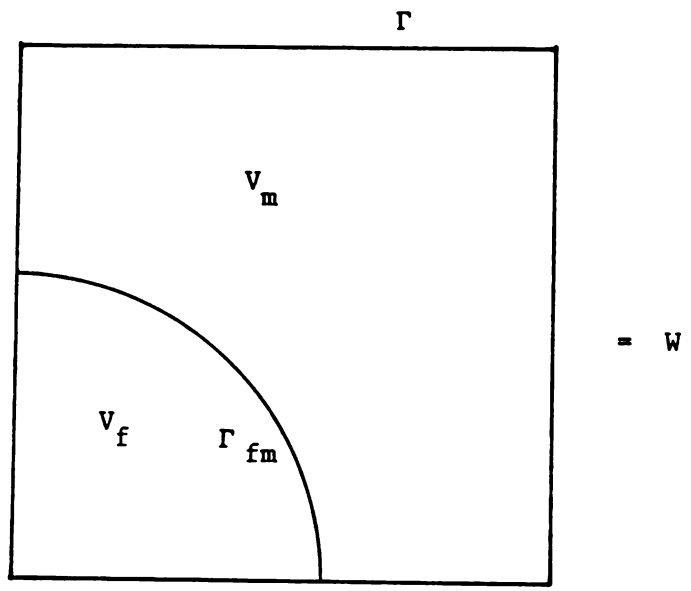

(a)

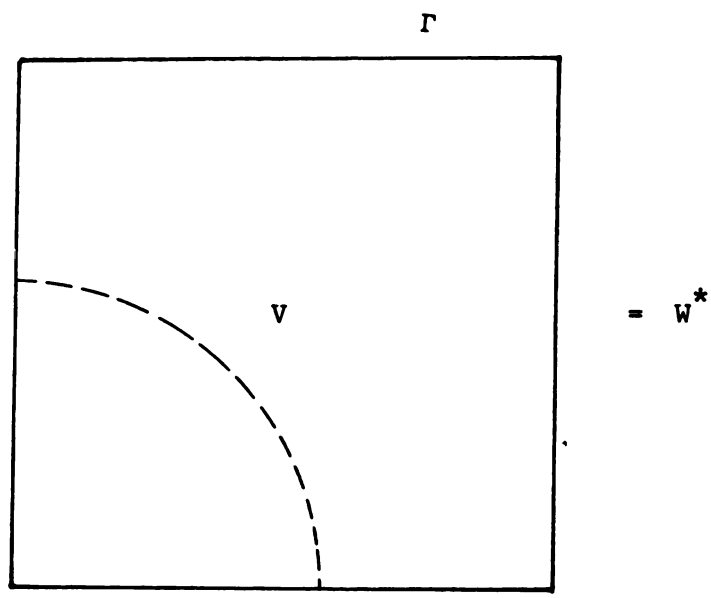

(b)

Figure 4.1. Fundamental units of (a) heterogeneous fiber/matrix composite and (b) macroscopically homogeneous composite

In the presence of possible discontinuities in the displacement field across Γ_{fm}, the work done in the fiber/matrix composite is

$$W = \frac{1}{2}\int_{\Gamma} u_i\, t_i\, d\Gamma = \frac{1}{2}\int_{V} \sigma_{ij}\, \epsilon_{ij}\, dV - \frac{1}{2}\int_{\Gamma_{fm}} [u]_i\, t\ \ d\Gamma_i \tag{4.2}$$

where the last integral of equation (4.2) represents an internal "interface work" due to the displacement discontinuity across Γ_{fm}.

If the same displacement boundary conditions are imposed on the two media, i.e. $u_i^*(\Gamma) = u_i(\Gamma) = u_i^0(\Gamma)$, the work done on the two media must be equal i.e.

$$\int_{\Gamma} u_i^0\, t_i^*\, d\Gamma = \int_{\Gamma} u_i^0\, t_i\, d\Gamma \tag{4.3}$$

or

$$\int_{\Gamma} u_i^0\, \sigma_{ij}^* n_j\, d\Gamma = \int_{\Gamma} u_i^0\, C_{ijkl}^*\, \epsilon_{kl}^0 n_j\, d\Gamma$$

$$= C_{ijkl}^* \int_{\Gamma} u_i^0\, \epsilon_{kl}^0\, n_j\, d\Gamma = \int_{\Gamma} u_i^0\, t_i\, d\Gamma \tag{4.4}$$

where $\sigma_{ij}^* = C_{ijkl}^*\, \epsilon_{kl}^0$. (4.5)

4.2 Statistically transversely isotropic effective composites

We assume here, for simplicity, that the effective homogeneous medium can be characterized as transversely isotropic. Let x_1 be oriented along the fiber direction. Then the stress-strain relation can be written in the form

$$\sigma_{11}^* = C_{11}^* \epsilon_{11}^0 + C_{12}^* \epsilon_{22}^0 + C_{12}^* \epsilon_{33}^0$$

$$\sigma_{22}^* = C_{12}^* \epsilon_{11}^0 + C_{22}^* \epsilon_{22}^0 + C_{23}^* \epsilon_{33}^0$$

$$\sigma_{33}^* = C_{12}^* \epsilon_{11}^0 + C_{23}^* \epsilon_{22}^0 + C_{22}^* \epsilon_{33}^0$$

$$\sigma_{12}^* = 2 C_{66}^* \epsilon_{12}^0$$

$$\sigma_{23}^* = (C_{22}^* - C_{23}^*) \epsilon_{23}^0$$

$$\sigma_{31}^* = 2 C_{66}^* \epsilon_{31}^0 \qquad (4.6)$$

where the five constants C_{11}^*, C_{12}^*, C_{22}^*, C_{23}^* and C_{66}^*, designate the five independent effective properties of the medium. Hashin [65] introduced the convenient engineering properties, plane strain bulk modulus K_{23}^*, Young's modulus E_{11}^*, shear moduli G_{12}^*, G_{23}^* and Poisson's ratio ν_{12}^* as follows

$$C_{11}^* = E_{11}^* + 4\nu_{12}^{*2} K_{23}^*$$

$$C_{12}^* = 2K_{23}^* \nu_{12}^*$$

$$C_{22}^* = G_{23}^* + K_{23}^*$$

$$C_{23}^* = - G_{23}^* + K_{23}^*$$

$$C_{66}^* = G_{12}^*. \qquad (4.7)$$

Other important elastic properties, transverse Young's modulus E_{23}^* and transverse Poisson's ratio ν_{23}^*, are related to the moduli in equations (4.7) by

$$E_{23}^* = \frac{4 K_{23}^* G_{23}^*}{K_{23}^* + \Psi G_{23}^*} = 2(1+\nu_{23}^*)G_{23}^* \qquad (4.8)$$

$$\nu_{23}^{*} = \frac{K_{23}^{*} - 4G_{23}^{*}}{K_{23}^{*} + \Psi G_{23}^{*}} \tag{4.9}$$

where

$$\Psi = 1 + \frac{4K_{23}\nu_{12}^{*2}}{E_{11}^{*}} \tag{4.10}$$

Elastic moduli G_{23}^{*} and K_{23}^{*} of the statistically transversely isotropic effective composite can be determined by equations (4.4-8) with prescribed displacement as shown in Figure 4.2.

A) Effective plane strain bulk modulus K_{23}^{*}

Consider a state of biaxial strain specified by $u_2^0 = u^0 = u^0 = 1$ at $x_2 = 1$, $u_3^0 = u^0 = u^0 = 1$ at $x_3 = 1$ and $u_1^0 = 0$. Then from equations (4.1), (4.6) and (4.7), the work done on the effective medium is

$$W^{*} = \int_{\Gamma} u_i^0 \; t_i^{*} \, d\Gamma = \int_{\Gamma_{ABCD}} u_i^0 \, \sigma_{ij}^{*} n_j \, d\Gamma = \int_{\Gamma_{BC}} u_2^0 \, \sigma_{22}^{*} d\Gamma + \int_{\Gamma_{CD}} u_3^0 \, \sigma_{33}^{*} d\Gamma$$

$$= \int_{\Gamma_{BC}} u_2^0 (C_{22}^{*} \epsilon_{22}^0 + C_{23}^{*} \, \epsilon_{33}^0) d\Gamma + \int_{\Gamma_{CD}} u_3^0 (C_{23}^{*} \epsilon_{22}^0 + C_{22}^{*} \, \epsilon_{33}^0) d\Gamma.$$

From the boundary conditions $u_2^0 = u_3^0 = 1$ and equations (4.7) and (4.3), the work done on the two systems are equivalent i.e., $W^{*} = W$. Thus

$$W^{*} = \int_{\Gamma_{BC}} 2K_{23}^{*} d\Gamma + \int_{\Gamma_{CD}} 2K_{23}^{*} d\Gamma = W = \int_{\Gamma_{ABCD}} t_i \, d\Gamma.$$

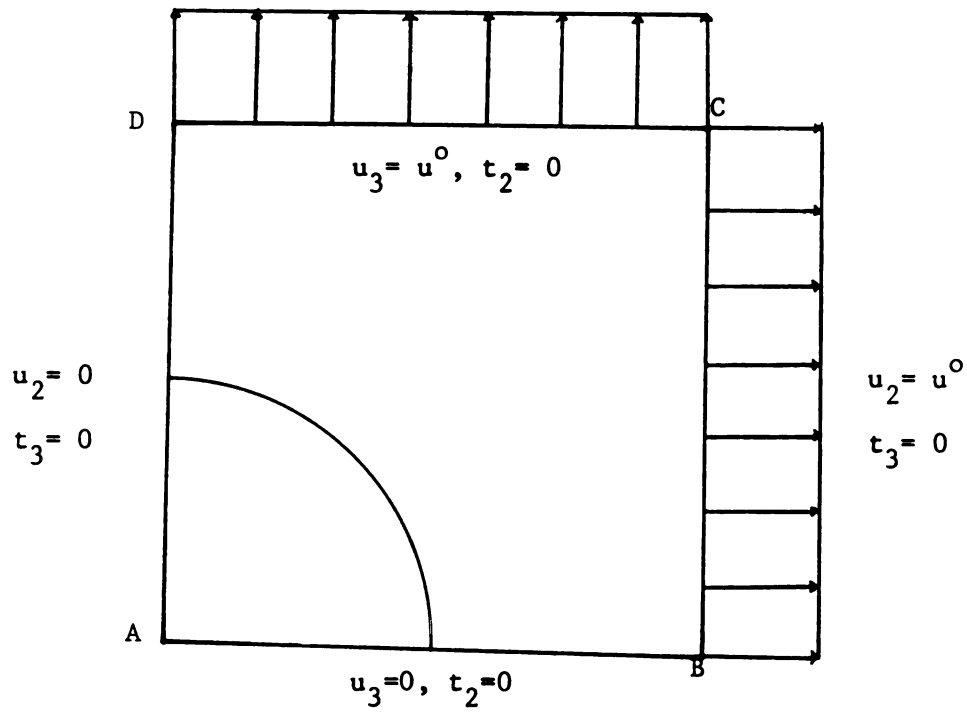

(a)

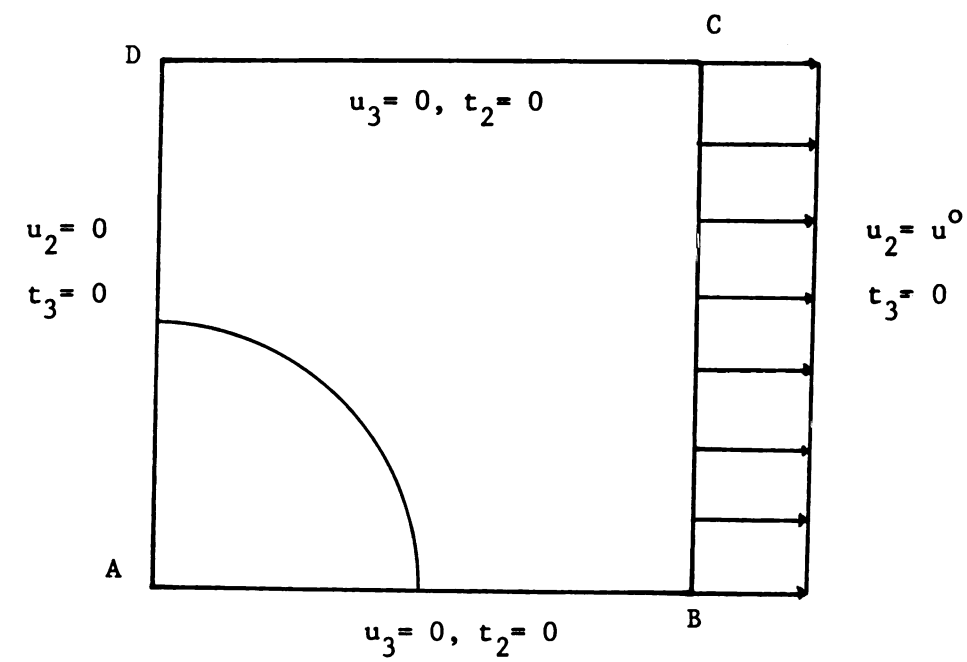

(b)

Figure 4.2. Boundary conditions for (a) biaxial tension and (b) uniaxial tension

B) Effective Transverse shear moduli G_{23}^*

Next consider the state specified by $u_2 = u^0 = 1$ at $x_2 = 1$ and all other normal displacements $u_i = 0$. The work done on the effective medium is

$$W^* = \int_\Gamma u_i^0 \, t_i^* \, d\Gamma = \int_{\Gamma_{ABCD}} u_i^0 \, \sigma_{ij}^* \, n_j \, d\Gamma = \int_{\Gamma_{BC}} u_2^0 \, (C_{22}^* \, \epsilon_{22}^0) \, d\Gamma$$

similarly, from equations (4.7) and (4.3), the work done on the effective and composite media are equivalent so that

$$W^* = \int_{\Gamma_{BC}} u_2^0 (K_{23}^* + G_{23}^*) d\Gamma = W = \int_\Gamma u_i^0 \, t_i \, d\Gamma.$$

With K_{23}^* calculated using the previous boundary conditions, one can now determine the transverse shear modulus G_{23}^*.

In order to obtain other effective elastic moduli for transversely isotropic phase, it is very convenient to use Hill's relations [16]. Hill has shown that for a unidirectional fibrous two-phase material with transversely isotropic phases

$$E_{11}^* = \bar{E}_{11} + \frac{4(\nu_f - \nu_m)^2}{\left(\frac{1}{K_f} - \frac{1}{K_m}\right)^2} \left(\frac{\bar{1}}{K} - \frac{1}{K^*} \right) \tag{4.11}$$

$$\nu_{12}^* = \bar{\nu}_{12} - \frac{(\nu_f - \nu_m)}{\left(\frac{1}{K} - \frac{1}{K}\right)} \left(\frac{\bar{1}}{K} - \frac{1}{K^*} \right) \tag{4.12}$$

where

$$\bar{E}_{11} = E_f V_f + E_m V_m \tag{4.13}$$

$$\bar{\nu}_{12} = \nu_f V_f + \nu_m V_m . \tag{4.14}$$

Since K^*_{23} for a transversely isotropic phase is determined by the previous analogy, effective axial moduli E^*_{11} and ν^*_{12} will be obtained from equations (4.12-13). The transverse isotropic effective moduli E^*_{23} and ν^*_{23} can be determined from equations (4.9-11).

4.3 Damaged interfacial behaviors

In the process of forming the material, the properties of the constituents themselves may be altered because of a variety of factors, including preferential surface absorption, catalytic effects on the chemical reaction between constituents and different thermal effects [66]. In general, one may say that there is some theoretical maximum bond strength that can be developed under ideal conditions of perfect molecular contact. However, the primary loss of strength is due to failure of the molecules to approach their proper bonding distances. One may visualize this as microvoids and microcracks at the interface. A second major loss in bond strength comes about from the development of residual stresses at the interface. Normally, a 'matrix' or 'adhesive' is applied in the fluid state and then solidified by cooling and/or chemical reaction. This invariably causes a differential shrinkage at phase boundaries that leads to undesirable stress concentration. The deviation stresses which act tangential to interfaces in composite systems can lead to interface failure under

certain conditions and this is one of the control problems of composite processing [66].

In a brittle matrix composite, cracks can form either within or around the particles of the dispersed phase during fabrication due to the difference in the thermal contractions of the two phase. The location and geometry of the cracks depends on the stress distribution and the fracture energy of each phase [51,52].

The residual thermal stresses will induce cracks and fracture paths as shown in Figure 4.3. For the case where thermal expansion coefficient $\alpha_p > \alpha_m$, either hemispherical cracks will form around the particle when fracture energy $\gamma_p > \gamma_m$. Cracks can also form at the particle/matrix interface when the fracture energy of the interface is lower than both that of the particle and matrix phase. This occurs for poor interfacial bonding. For the case $\alpha_m > \alpha_p$, radical cracks develop regardless of the fracture energy of the two phases. Binns [67] and Evans [52] observed that of the cracks shown in Figure 4.3, the radial cracks were most detrimental since they may easily link together and form a network of interparticle cracks.

The non-symmetric stress distribution due to the different elastic properties of the two phase must also be considered since, for most composite, the cracks associated with the particles form during stressing as shown in Figure 4.4. Unless the thermal expansion coefficients of both phases are equal, these more complex stress distributions must be superimposed on residual stress distributions to

From ref. 53

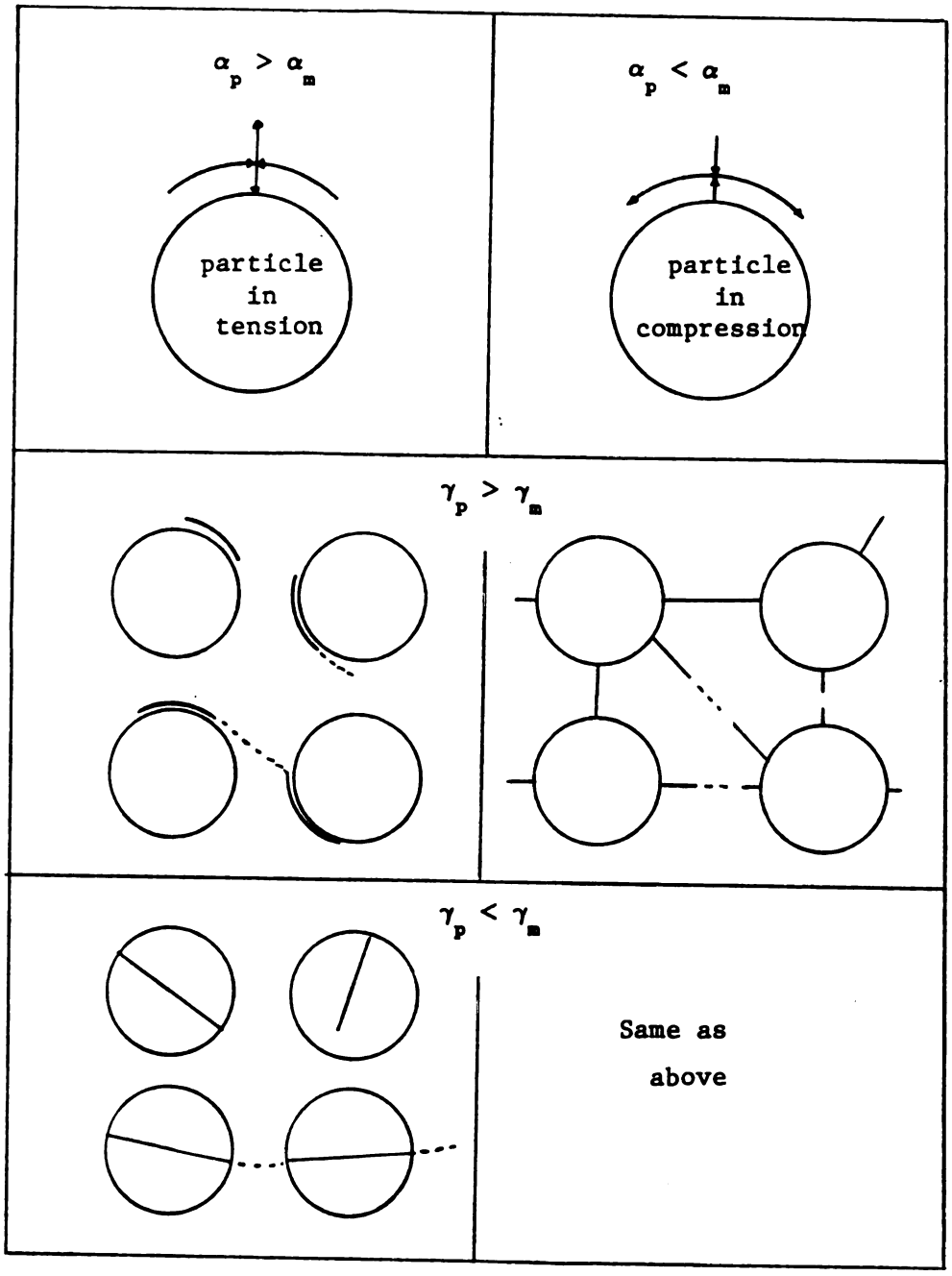

Figure 4.3. Nature of residual thermal stress, crack location, and fracture path (broken lines)

From ref. 53

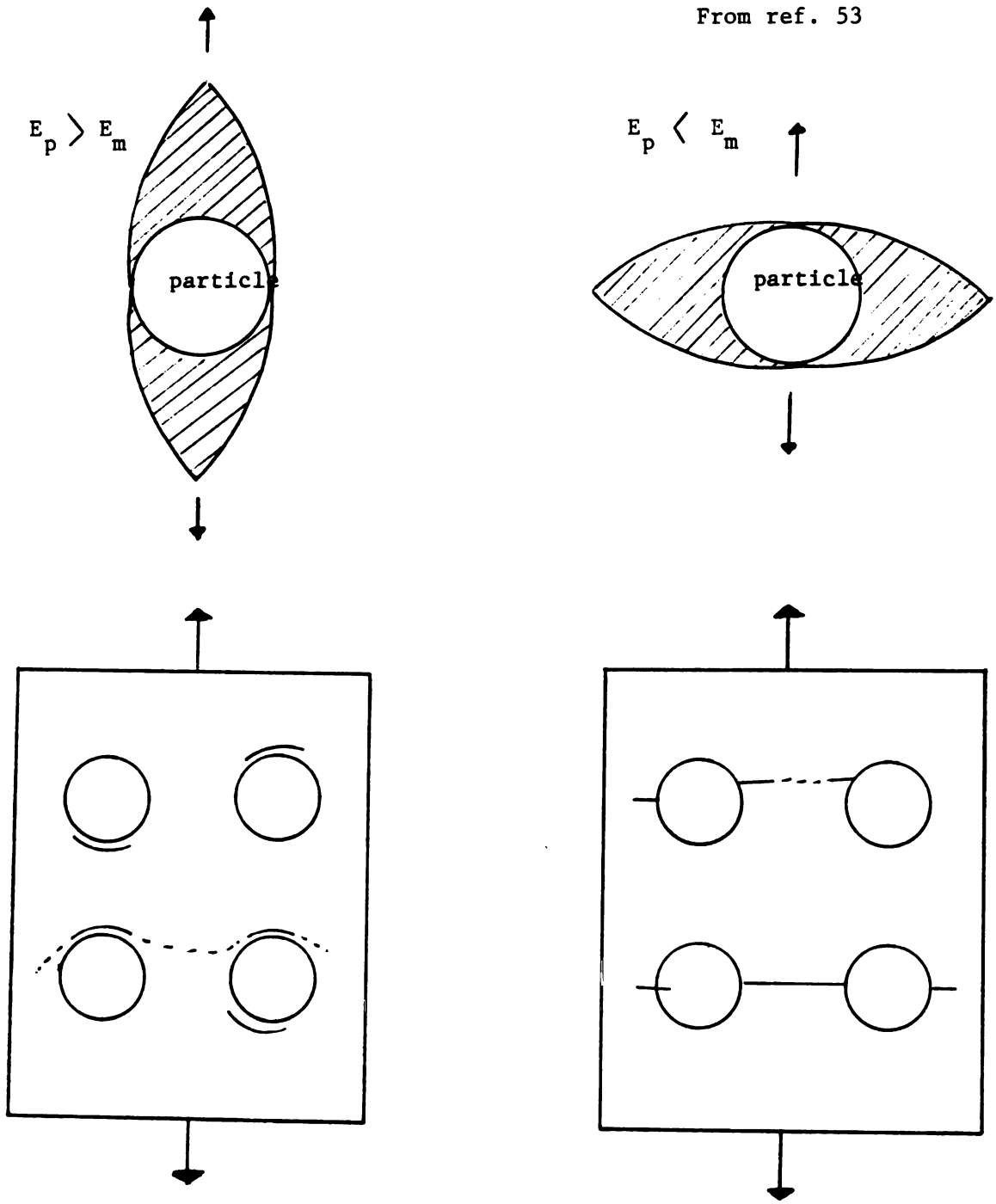

Figure 4.4. Schematic of the enhanced tensile stresses around spherical particles. The location of cracks and fracture path (broken lines)

obtain crack locations and fracture modes.

Although no direct technique has been developed to determine the crack size due to the thermal residual stresses and differential elastic moduli of the two phase, in this analysis we introduce the simple micro-crack density parameter to estimate the effective elastic moduli of the fiber-reinforced composite.

In the estimation of effective elastic moduli for improper interface-bonding materials, we will introduce the interphase degradation model and tangential displacement discontinuity model. For simplicity, we assume that debonded region will occur only at the fiber/matrix interface.

4.3.1 Interphase degradation model

Let's consider a third phase between the fiber and matrix as shown in Figure 4.5. The existence of an interphase layer has been demonstrated by infra-red spectroscopy, ESP, NMR, electron microscopy and other experimental methods [49,50]. It has also been shown that the thickness of this layer depends on the polymer cohesion energy, free surface energy of the solid and the flexibility of the polymer chains. However, the thickness of the interphase has been shown to be very small in comparison with the size of the two constituent materials.

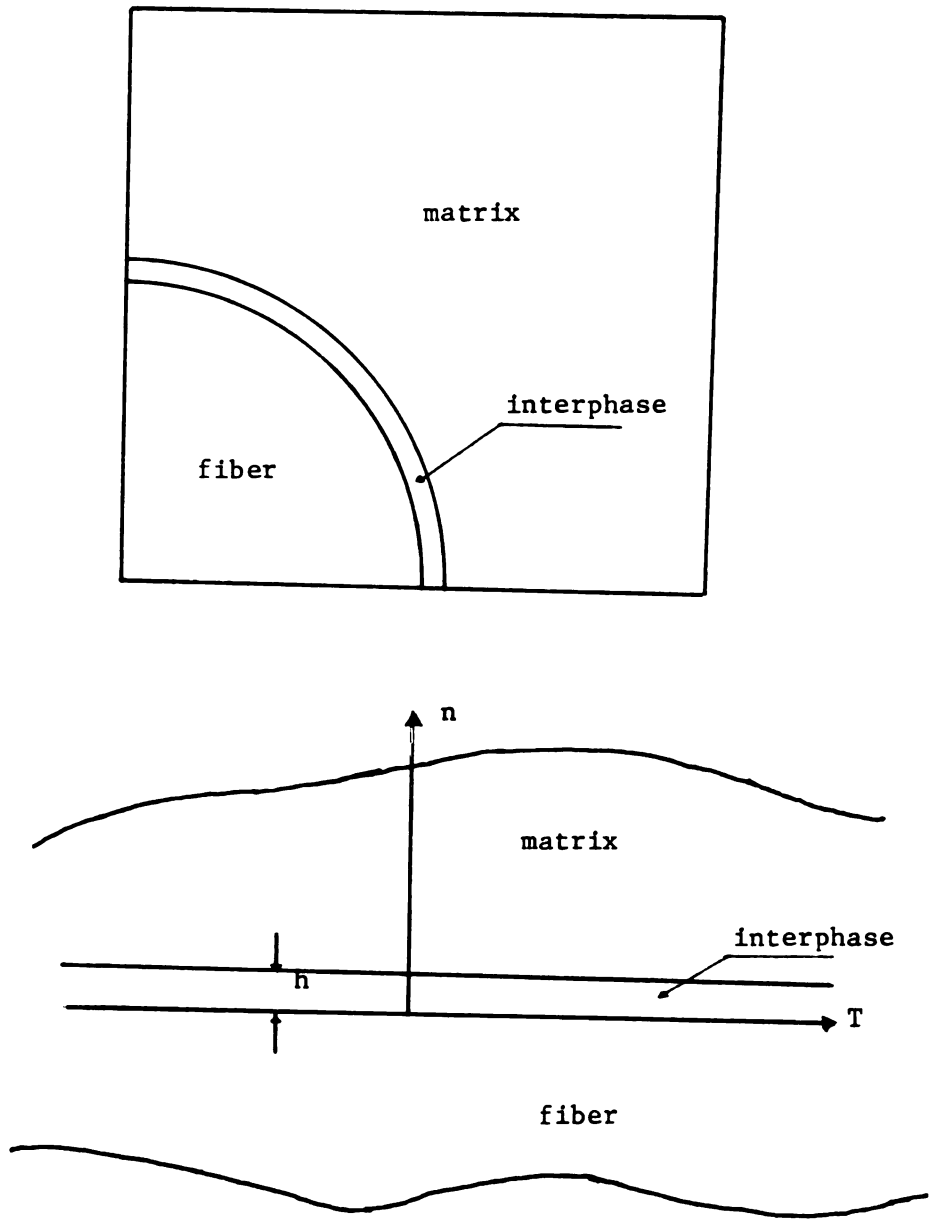

Figure 4.5. Thin interphase BEM model

To apply the B.E.M subregional technique, the interphase layer has to be discretized into elements small enough to ensure that nodes on opposite interfaces are sufficiently distant from each other in comparison with the size of the boundary elements. Otherwise, numerical inaccuracies will arise.

An alternative scheme to improve the boundary element formulation consists of finding a relationship between the points on opposite faces of the thin layer [68]. Consider the thin layer and apply one-dimensional stress-strain relationships for shear and compression in a finite difference manner. If the thickness of the layer element, h, is small by comparison with the boundary element lengths, one can write

$$t_n^{(f)} = \left(u_n^{(f)} - u_n^{(m)} \right) \frac{E_{inter}}{h}$$

$$t_t^{(f)} = \left(u_t^{(f)} - u_t^{(m)} \right) \frac{G_{inter}}{h}. \qquad (4.15)$$

where E_{inter} and G_{inter} are Young's and shear moduli respectively of the interphase material and the displacements are referred to the local system of coordinates indicated in Figure 4.5. Two other relationships are provided by the equilibrium conditions i.e., $t_i^{(f)} + t_i^{(m)} = 0$.

In the interphase model, the effects of improper interfacial bonding strength can be easily considered as the degradation of elastic properties in the interphase region. When the elastic properties of the interphase is equal to those of the matrix, it is

considered as a perfect bond. However, when microcracks or voids are formed in the interphase due to the thermal residual stresses, one may expect that the interphase elastic properties will be less than those of the surrounding matrix. For simplicity, we assume that micro-cracks only occur in the interphase region and other two constituent materials perform their inherent elastic properties. Then the degradation of interphase elastic properties can be calculated from micro-crack density κ.

We assume that the cracks are uniformly distributed with a characteristic density β and an average crack length L in the interphase region as shown in Figure 4.6. Thus, if A is any area which is large compared to L^2, this area should contain $A\beta$ cracks regardless of the location or geometry of the region A. Since we assume the cracks are mechanically independent, this approximation is valid for a lightly cracked material. The model is defined by two geometric parameters: a length L and an inverse area α ($= A^{-1}$). Walsh [69] examined these parameters to describe certain lightly cracked rock materials.

Using the known solution for displacements at a crack [70], we can calculate the interface work of equation (4.2) as

$$\Delta W = \int_{\Gamma_{cracked}} [u]_i t \; d\Gamma_i = 2\pi\kappa(1-\nu)(\sigma_2^2 + \sigma_3^2)/E_{23}^2 \qquad (4.16)$$

where $\kappa = \alpha L^2$ is the dimensionless measure of crack density and E is Young's modulus of an uncracked homogeneous and isotropic matrix body.

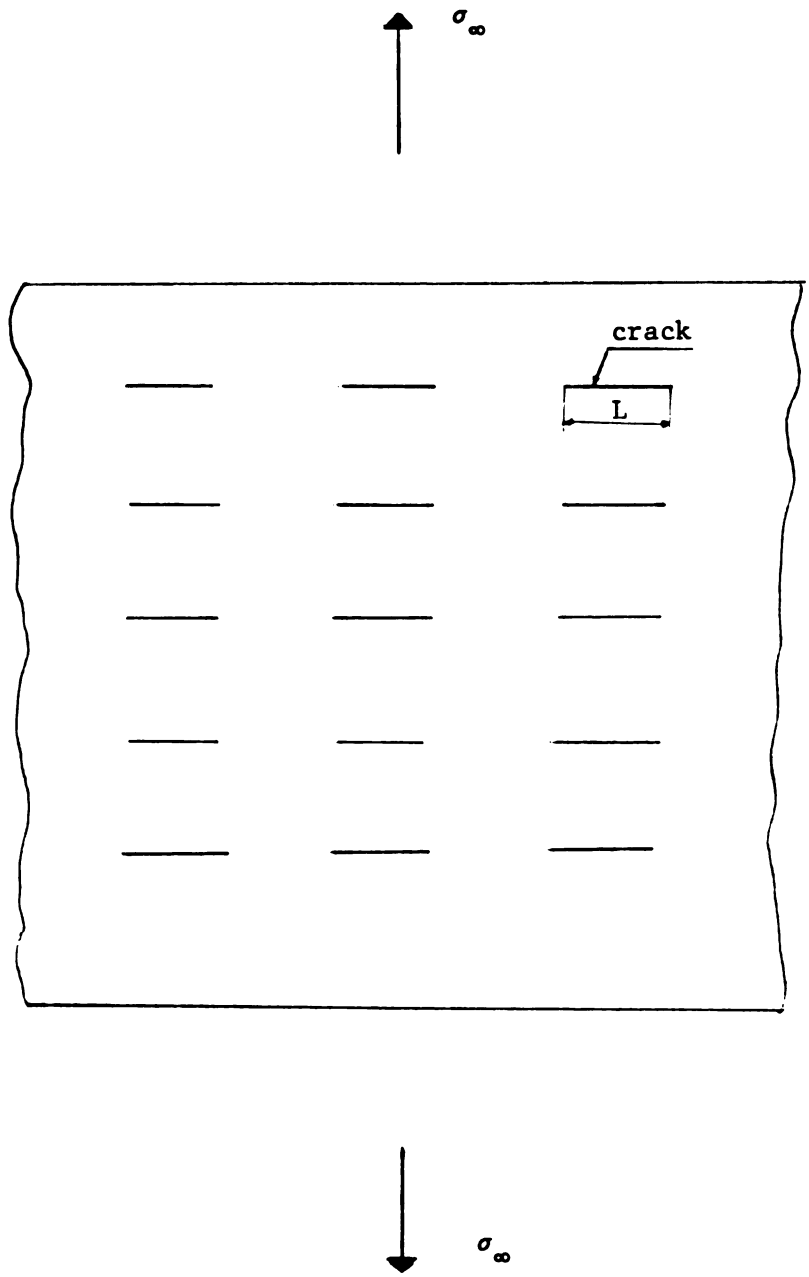

Figure 4.6. Line cracked material model

The average stress-strain relations corresponding to the strain energy of cracked material is [70]

$$\epsilon_2 = \frac{1}{E}\{\sigma_2 - \nu(\sigma_3 + \sigma_1)\}$$

$$\epsilon_3 = \frac{1}{E}\{\sigma_3 - \nu(\sigma_2 + \sigma_1)\} + 2\pi\kappa(1-\nu^2)\sigma_3/E$$

$$\epsilon_{23} = \frac{1+\nu}{E}\sigma_{23} + 2\pi\kappa(1-\nu^2)\sigma_{23}/E. \qquad (4.17)$$

They have the effect of making the overall mechanical response anisotropic, i.e.

$$\epsilon_2 = \frac{1}{E_2}\{\sigma_2 - \nu_{23}\sigma_3\}$$

$$\epsilon_3 = \frac{1}{E_3}\{\sigma_3 - \nu_{32}\sigma_2\}$$

$$\epsilon_{23} = \frac{1}{G_{23}}\sigma_{23} \qquad (4.18)$$

where

$$E_2 = E$$

$$E_3 = E/(1+2\pi\kappa(1-\nu^2))$$

$$\nu_{23} = \nu_{32} = \nu$$

$$G_{23} = G/(1+2\pi\kappa(1-\nu^2)) \qquad (4.19)$$

Due to the thermal and mechanical properties of two the constituents, more complex cracks will be formed. For simplicity, we assume the overall cracked material to be isotropic in the sense of an average response.

4.3.2 Tangential displacement discontinuity model

Due to several damage phenomena, some separation may exist between the constituents at their interface. This debonding is certainly non-uniform in the composite. In order to model the complicated effect of debonding on the thermo-mechanical behavior of the composite, it is necessary to introduce a relaxation of the tangential displacement continuity condition, which simulates separation at the interface [27,28]. The partial discontinuity model is that in which the continuity of the normal displacements and tractions prevail at the fiber/matrix interface. However, some degree of slip, reflected by a jump in the tangential displacement is allowed. Thus

$$[\,\sigma_{ij}\,]\,n_j = 0$$

$$[\,u_i\,]\,n_i = 0 \qquad \text{on } \Gamma_{interface} \tag{4.21}$$

where $[\,\bullet\,]$ denotes the jump of the bracketed expression across the interface, but

$$[u_t] = R\,t_t \qquad \text{on } \Gamma_{interface} \tag{4.22}$$

where u_t and t_t are the tangential displacement and shear traction vector respectively. R is a constant of proportionality, which represents the degree of bond or lubrication at the interface. Note that the usual case of perfect continuity is obtained by the limit condition $R \to 0$, while the case of lubricated sliding at the interface is obtained by $R \to \infty$. While, intermediate range, $0 < R < \infty$, this model demonstrates the certain damage state of composite behaviors.

Chapter 5

RESULTS AND DISCUSSION

5.1 Thermal residual stresses

Here we employ the superposition method to obtain a numerical approximation of the thermally-induced residual stresses during the curing process in the fundamental unit of a fiber-reinforced composite as shown in Figure 3.1. The thermal residual stresses at room temperature (21°C) after cool down from cure temperature (177 °C) were calculated using the boundary element analysis in conjunction with the S Glass/Hercules 3501-6 resin composite material properties listed in Table 5.1. Although the matrix material has temperature dependent properties [45], for simplicity, we assume that the matrix properties are constant throughout the cure process.

The predicted thermal residual stresses at the fiber/matrix interface for the S Glass/epoxy composite, assuming a fiber volume of 60 percent, are indicated in Figures 5.1 and 5.2. As can be seen in Figure 5.1, the normal stress σ_{rr} is primarily compressive, the highest values (σ_{rr} = -35.5 Mpa) occurring in the regions of closest fiber spacing. In the resin rich region, the normal stress is tensile although its magnitude is small (9.6 Mpa). The shear stress distribution is indicated in Figure 5.2. The highest interfacial shear

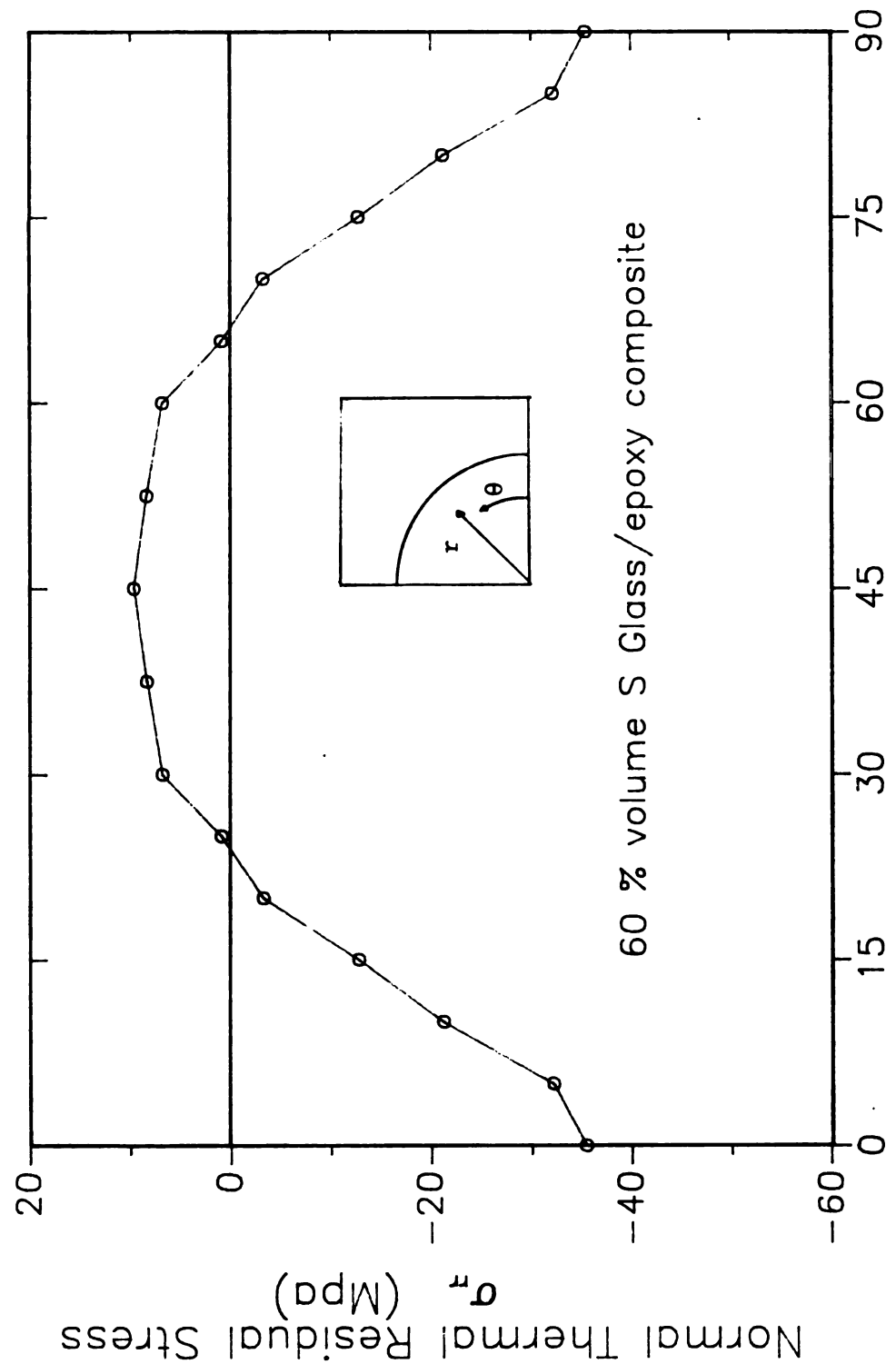

Figure 5.1. Normal thermal residual stress at the interface of a S Glass/epoxy composite (V_f= 60 %)

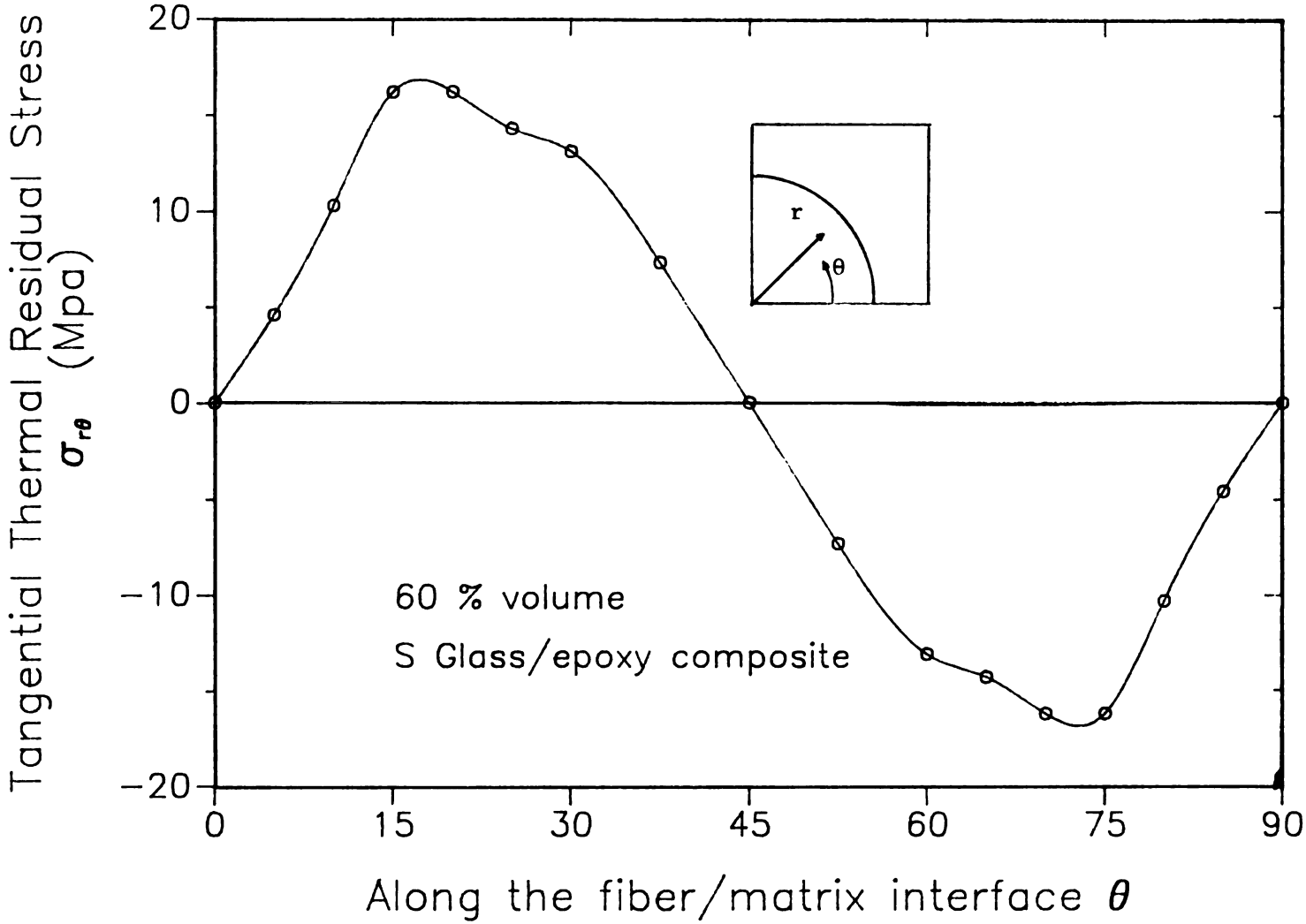

Figure 5.2. Tangential thermal residual stress at the interface of a S Glass/epoxy composite (V_f= 60 %)

stress is 15.5 Mpa. It will be noted that highest shear stresses do not occur at the same locations around the interface as the normal stresses. The present boundary element analysis is in good agreement with F.E.M [71] as shown in Table 5.2.

Table 5.1

Material properties of S Glass/epoxy composite constituents (Ref.71)

Materials	Properties
S Glass Fiber	E_f = 86 Gpa ν_f = 0.22 α_f = 5 x 10^{-6} °/ C
Hercules 3501 - 6 matrix	E_m = 4.3 Gpa ν_m = 0.34 α_m = 40 x 10^{-6} °/ C

Table 5.2

Comparison of thermal residual stresses at the fiber/matrix interface at room temperature (V_f = 60 percent)

	$\sigma_{rr\ Max}$	$\sigma_{rr\ Min}$	τ_{Max}	Node**
B.E.M	-35.5	9.6	15.4	70
F.E.M *	-31	10	13.5	230

* Adams [71] ** see Figure 3.2 units = Mpa

Figures 5.3 and 5.4 show the normal and tangential stress distributions at the three characteristic points A,B and C versus fiber volume fraction V_f. It can be seen from these figures that, at

the minimum interfiber distance, the stresses are compressive normal (radial) stresses and tensile tangential (hoop) stresses. There is a region around point C which is in a state of biaxial tension. The state of stress at point C is always hydrostatic tension since this point is an isotropic point.

It can also be deduced that an increase of V_f results in an increase of the compressive normal stress at point A. Koufopoulos and Theocaris [72] showed that this stress increases very rapidly for higher values of E_f/E_m. It is therefore expected that for some combination of high V_f and E_f/E_m, the compressive normal stress will exceed the strength of the matrix and initiate a crack. The tensile tangential stress at the point A decreases rapidly with increasing V_f. This stress may become compressive at $V_f \geq 70$ percent creating a biaxial compression at the point A.

A tensile normal stress is developed at point B when $V_f \geq 55$ percent. It is in fairly good agreement with a value of $V_f \geq 54$ percent in the case of rigid inclusion, given by Hsu [73] and $V_f \geq 49$ percent for $E_f/E_m = 2.4$ and $V_f \geq 54$ percent for $E_f/E_m = 11.4$ [72]. This tensile normal stress at the point B may initiate a bond crack at the interface. Since the tangential (hoop) stress distribution curve runs parallel to the normal stress distribution curve the tangential stress may also be large enough to initiate a crack in the radial direction.

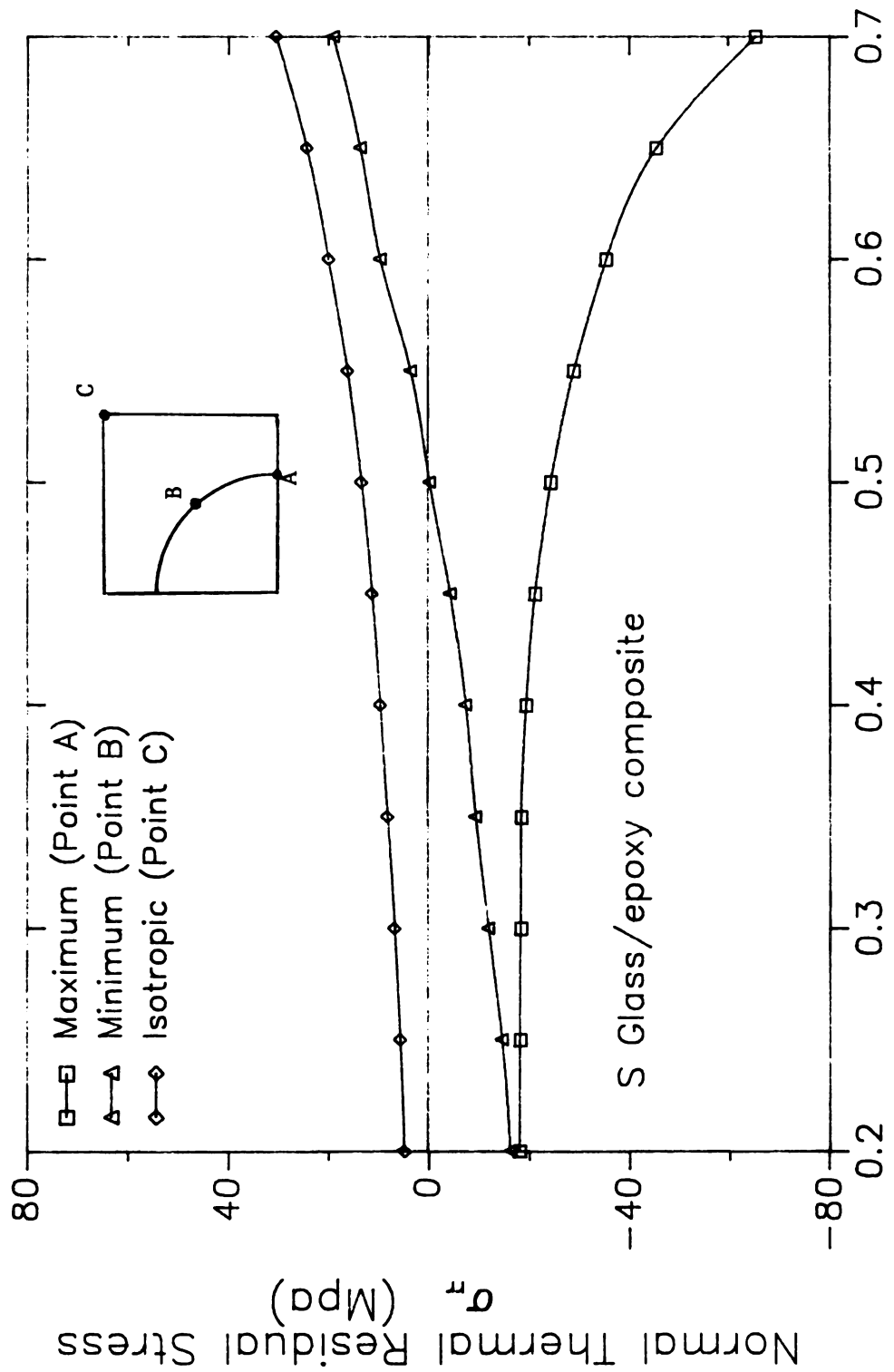

Figure 5.3. Normal thermal residual stresses at points A, B and C in a square array of fibers for a S Glass/epoxy composite

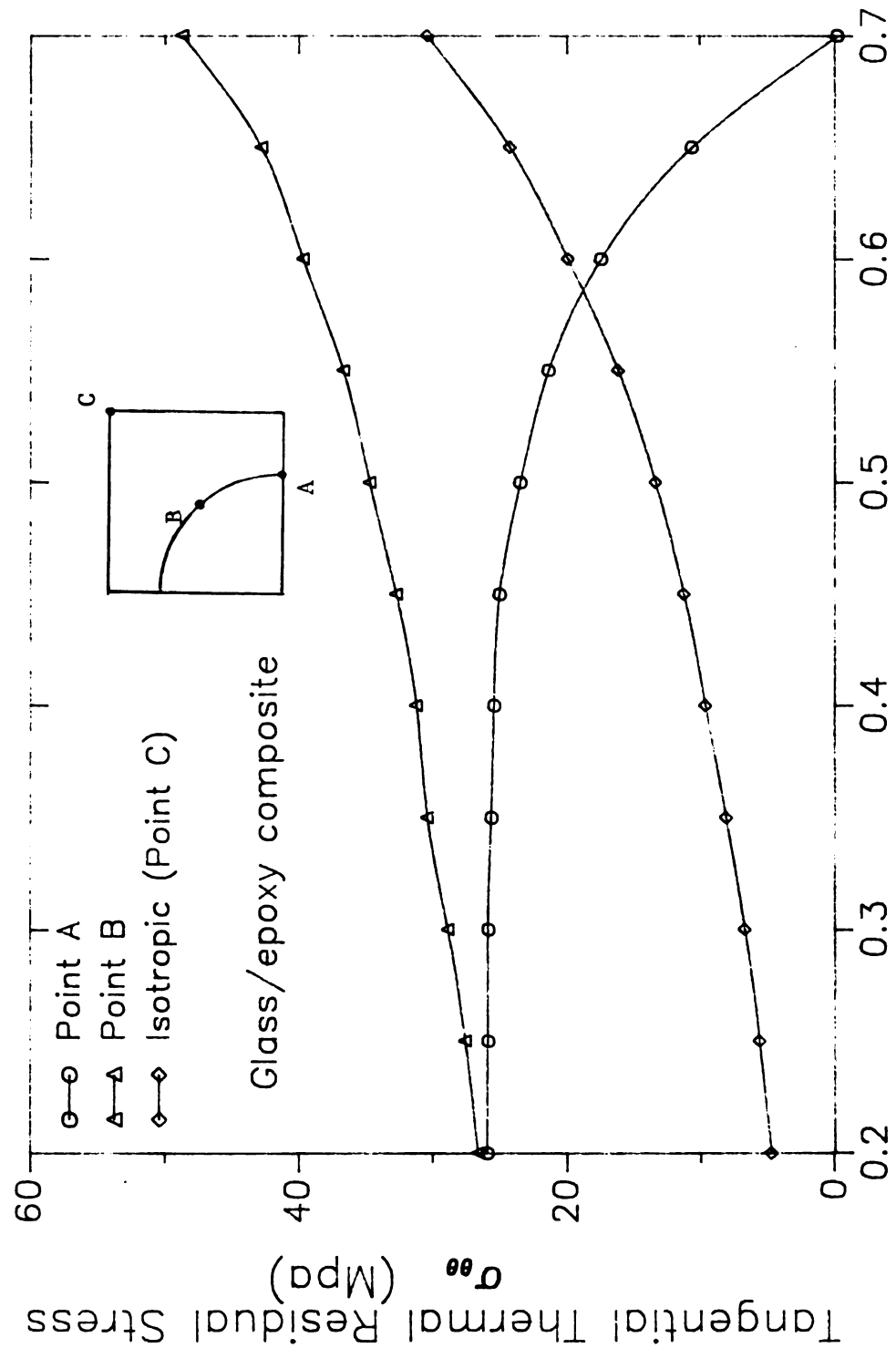

Figure 5.4. Tangential thermal residual stresses at points A, B and C in a square array of fibers for a S Glass/epoxy composite

5.2 Effective elastic constants

Among the five effective elastic properties of the equations 4.8 (K^*_{23}, E^*_{11}, ν^*_{12}, G^*_{12} and G^*_{23}) for the transversely isotropic medium, it has been shown to be very difficult to determine the transverse shear modulus G^*_{23} for the composite cylinder model [74]. The results for the effective transverse elastic moduli G^*_{23} and K^*_{23} of a composite material are shown in Figures 5.5 - 6. For the interface or interphase limiting case (perfect bonding), the effective moduli are plotted as a function of fiber volume fraction V_f. Calculations have been performed for a glass/epoxy composite (the constituent material properties are listed in Table 5.3) for V_f = 20, 30, 40, 50 and 60 percent.

Table 5.3

Material properties of the Glass/epoxy composite constituents (ref.16)

Materials	Properties
Glass fiber	$E_f = 10.5 \times 10^6$ psi $\nu_f = 0.2$
Epoxy resin	$E_m = 0.4 \times 10^6$ psi $\nu_m = 0.35$

In comparison to other analyses, the results of the present boundary element analysis are in good agreement for up to 50 percent fiber volume fraction. In fact, the effective plane strain bulk

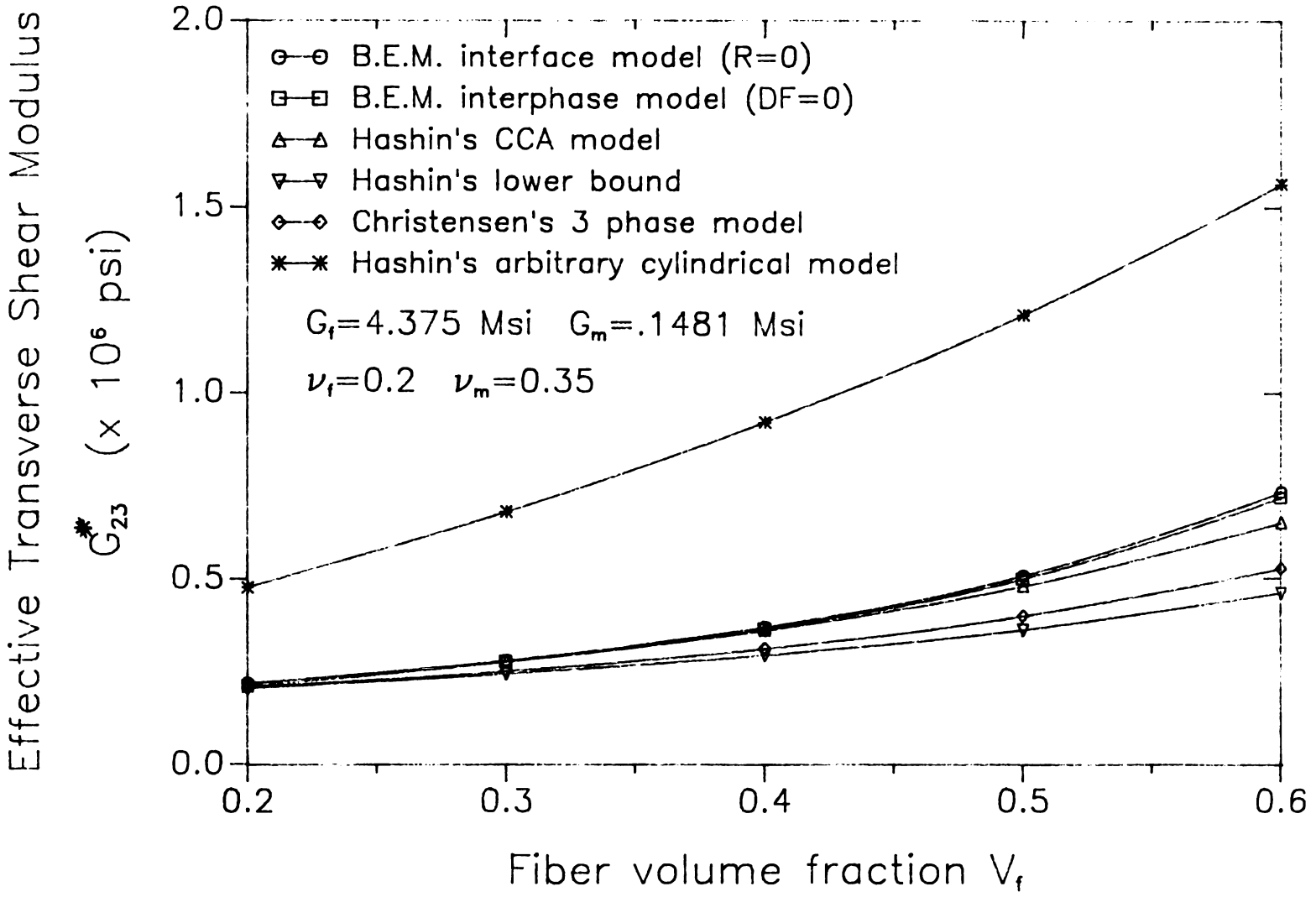

Figure 5.5. Effective transverse shear modulus G^*_{23} of the composite

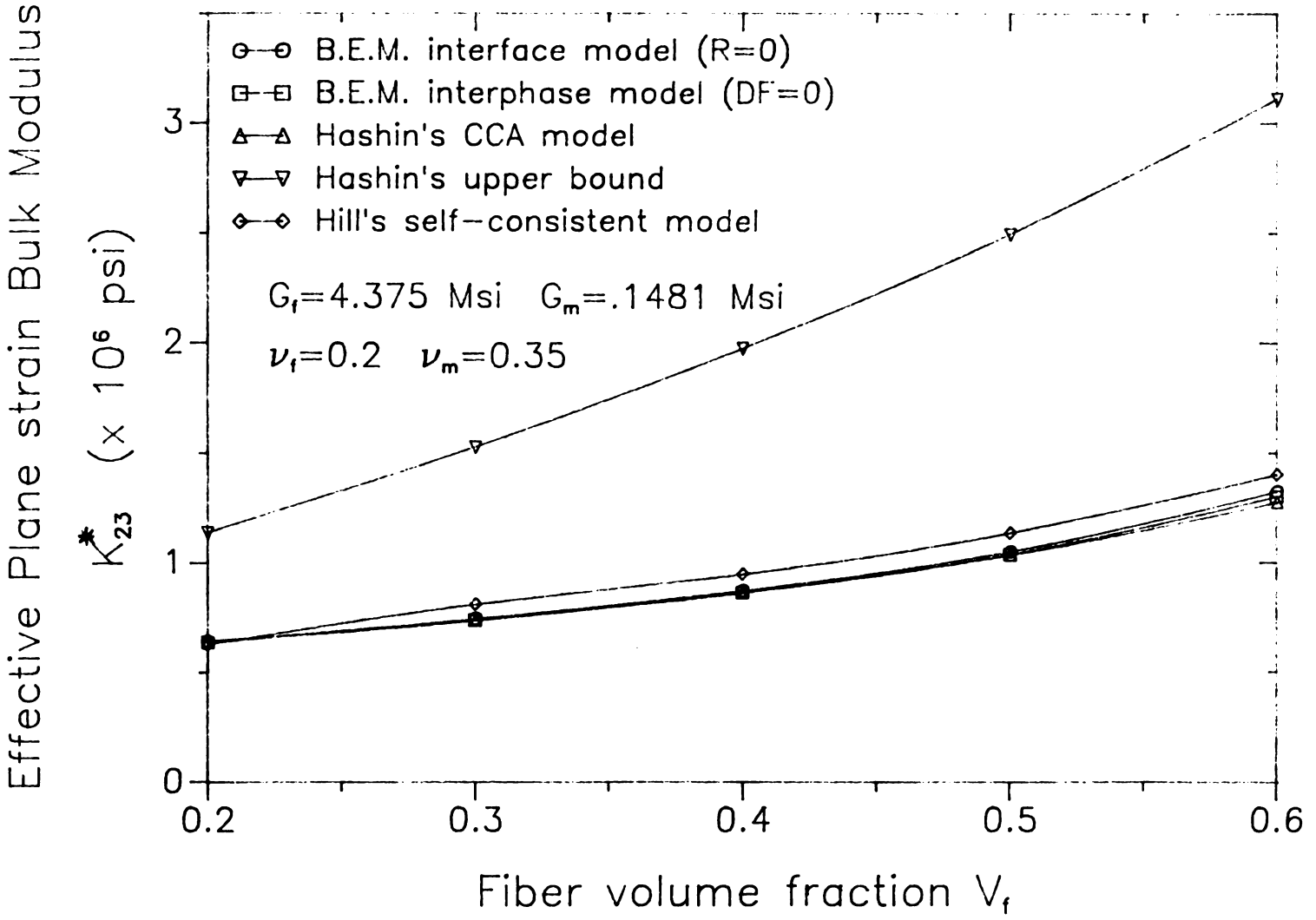

Figure 5.6. Effective plane strain bulk modulus K^*_{23} of the composite

modulus K_{23}^{*} is in an excellent agreement with Hashin's CCA model [65]for the entire range of volume fractions. For high V_f ($\geq$ 50%), the present square array model gives an effective transverse shear modulus G_{23}^{*} which is higher than those predicted by other (cylindrical) array analyses. A comparison with other analyses for G_{23}^{*} is given in Table 5.4. Figures 5.7 - 8 show that the transverse effective moduli E_{23}^{*} and ν_{23}^{*} are functions of fiber volume fraction V_f. E_{23}^{*} and ν_{23}^{*} of the present square array model are also in good agreement for up to 50 percent fiber volume fraction in comparison with Hashin's CCA model. According to Laws's investigation [75], the cylindrical array models under-estimate the transverse effective moduli G_{23}^{*} and E_{23}^{*} for the high fiber volume fraction composites ($V_f \geq$ 45%) in comparison with experiments, while ν_{23}^{*} is over-estimated. Adams and Doner [23] and Springer and Tsai [25] also showed that for higher V_f the square array's transverse effective moduli and effective thermal conductivity are in better agreement than those of the cylindrical square array.

It is also seen that the interface and interphase models are in excellent agreement with one another if elastic properties of the interphase are equal to those of the matrix (perfect bond). Since the interphase volume fraction is very small compared to that of the two constituents, the interphase region has little effect on the overall mechanical behavior . The values of the interphase thickness h and interphase volume fraction V_i for various fiber contents are given in Table 5.5 [50].

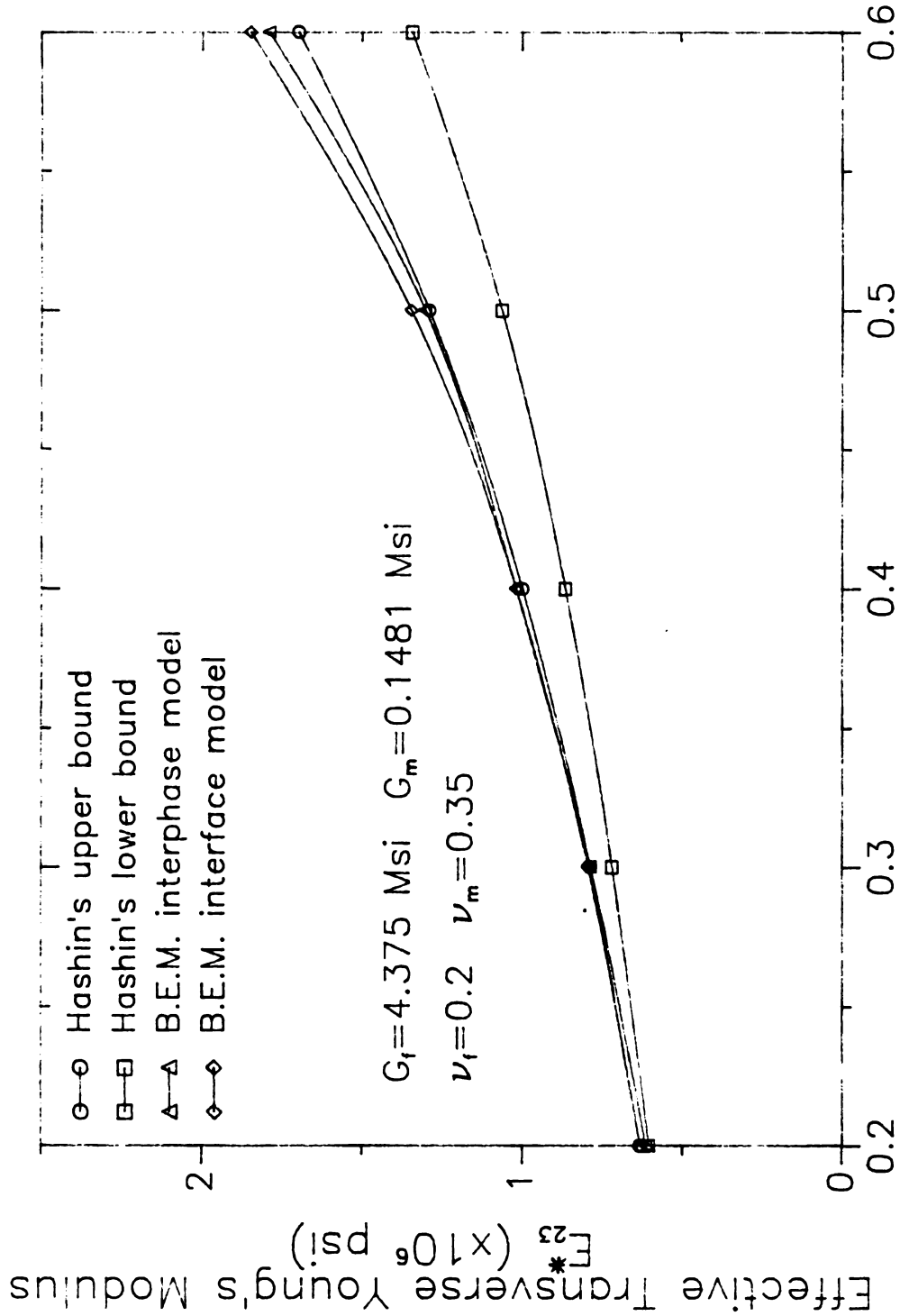

Figure 5.7. Effective transverse Young's modulus E_{23}^* of the composite

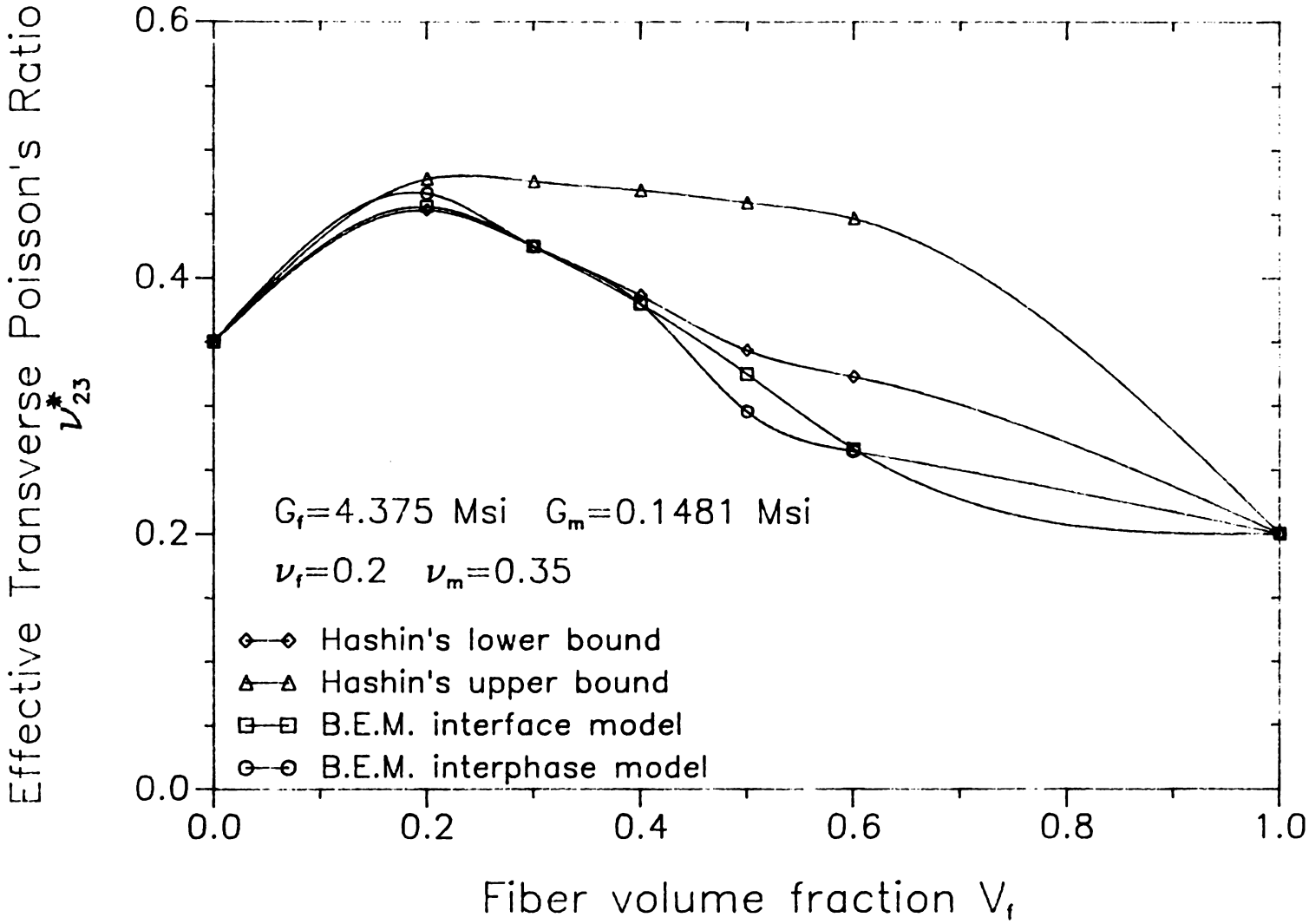

Figure 5.8. Effective transverse Poisson's ratio of the composite

Table 5.4

Comparison of Transverse shear modulus G_{23}^{*} with other analyses

units = 10^{6} psi

V_f	Inter-face	Inter-phase	Hashin's CCA	Hashin's lower	Christensen 3 phase
0.2	0.2125	0.209	0.2174	0.2043	0.2063
0.3	0.2787	0.2763	0.2765	0.2435	0.2505
0.4	0.3693	0.3656	0.3605	0.2946	0.3121
0.5	0.508	0.5036	0.4802	0.3642	0.4001
0.6	0.730	0.718	0.6525	0.4641	0.5293

Table 5.5

The thickness h and V_i for the interphase region (ref.50)

V_f	0.2	0.3	0.4	0.5	0.6
h	0.0109	0.0113	0.0177	0.0243	0.0315
V_i	0.005	0.011	0.020	0.031	0.044

Figures 5.9 shows the transverse shear modulus ratios versus V_f for various ratios G_f/G_m. It is shown that in the low range of volume fractions, the higher G_f/G_m ratio composites do not improve the effective transverse shear modulus.

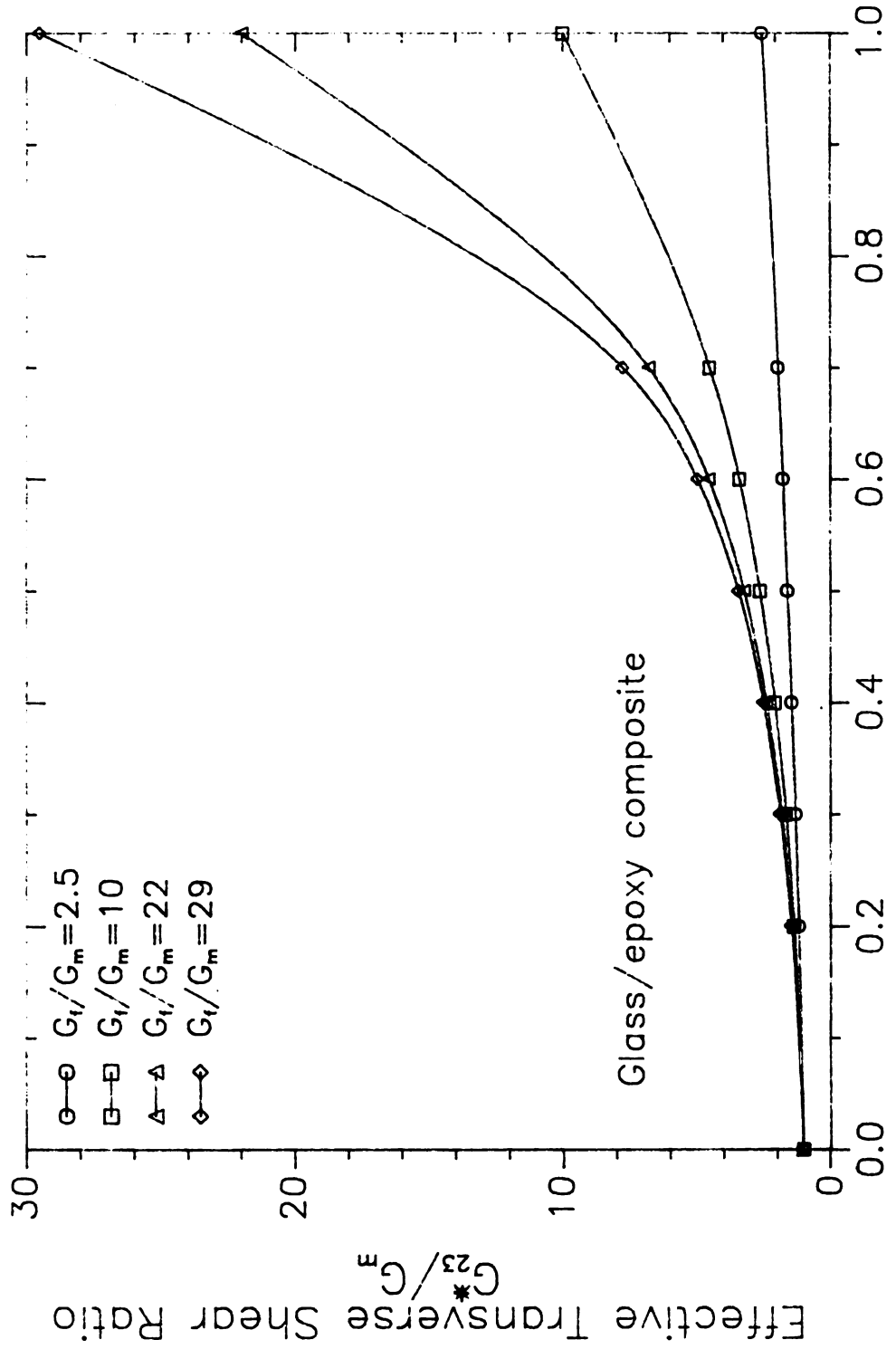

Figure 5.9. Effective transverse shear modulus ratios G^*_{23}/G_m for various fiber/matrix shear modulus ratios

5.3 The elastic behavior of damaged composites

The damage characteristics at the fiber/matrix interface due to thermal residual stresses, voids, and inherent micro-cracks may be too complex to describe by simple mathematical tools. Due to localized stress concentrations and micro-crack initiation, the damage is not uniformly distributed throughout the interfacial region. For simplicity, we here assume that the elastic moduli of the interphase region will be uniformly reduced due to the micro-crack density κ. As shown in Figure 5.10, the shear modulus is dramatically decreased with an increase in micro-crack density κ. In order to establish the shear modulus of the damaged interface, we represent the interphase condition using a degradation factor DF as shown in Figure 5.11. If there is no interphase damage (DF = 0), the shear modulus of the interphase will be the same as that of the matrix.

The results for the effective elastic moduli of the damaged-interphase composite are plotted in Figures 5.12 - 13. For small values of DF, the damage effects are not significant. The reason is that the micro-crack density κ increases steadily at low values of DF as shown in Figure 5.11. However, for high values of DF, the damage effects are severe. The effective elastic moduli, K_{23}^{*} and G_{23}^{*}, are dramatically decreased by an increase in DF. Figures 5.2.14 -15 also demonstrate that the damaged behavior of the effective shear and plane strain bulk moduli at 60 percent fiber volume fraction and various degradation factors DF.

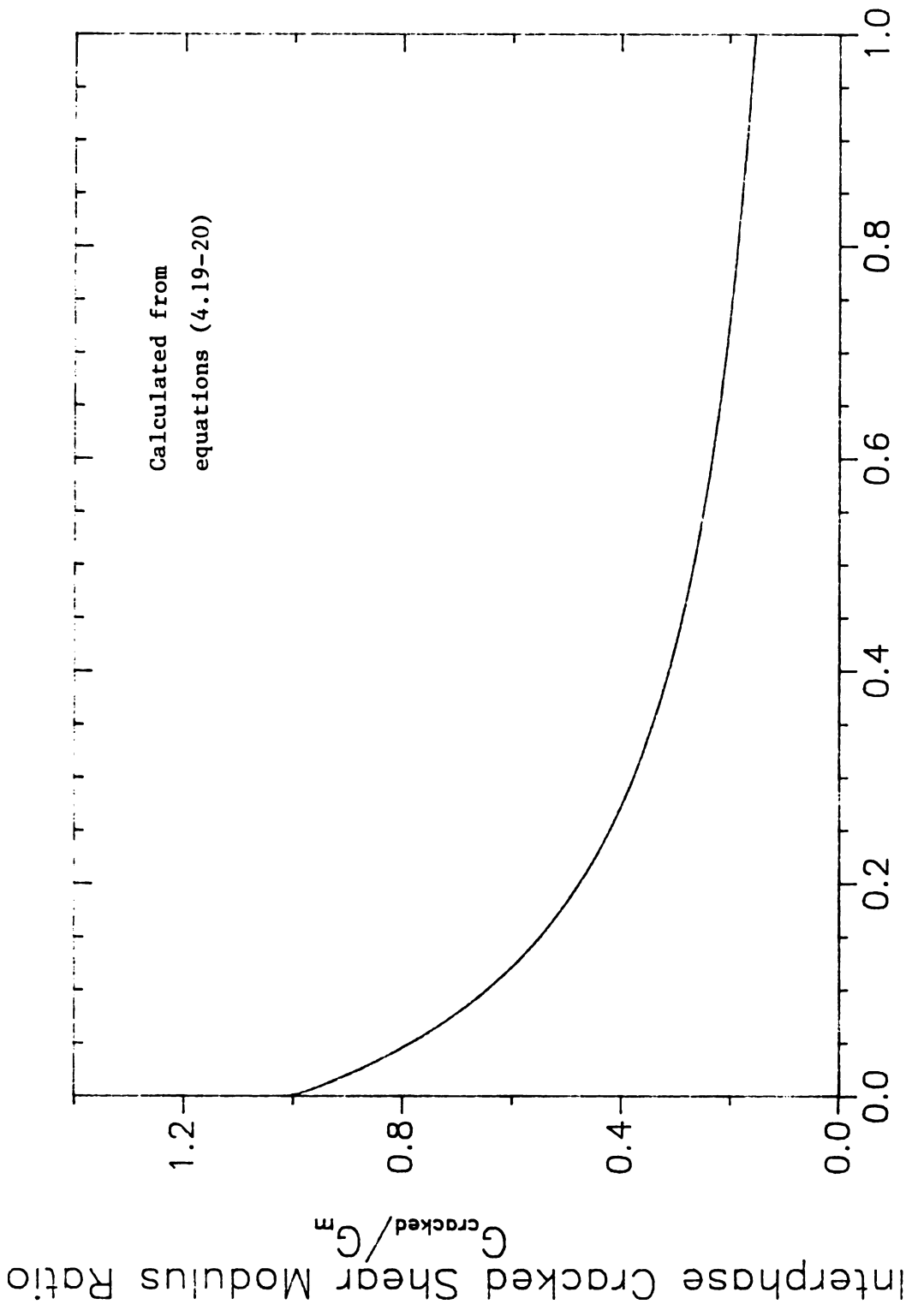

Figure 5.10. Cracked interphase shear modulus ratio $G_{cracked}/G_m$ due to micro-crack density k

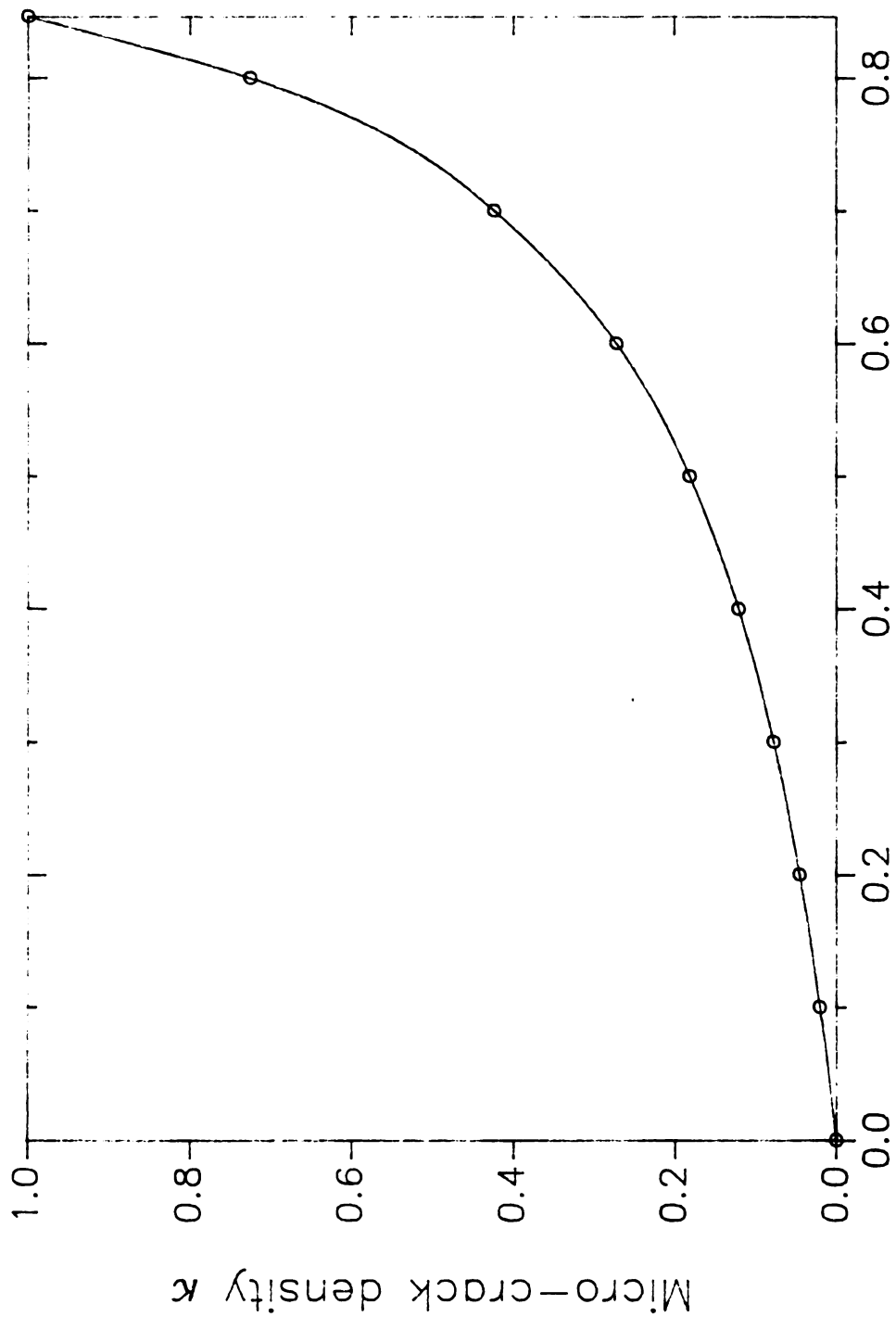

Figure 5.11. The relationship between micro-crack density k and interphase degradation factor DF

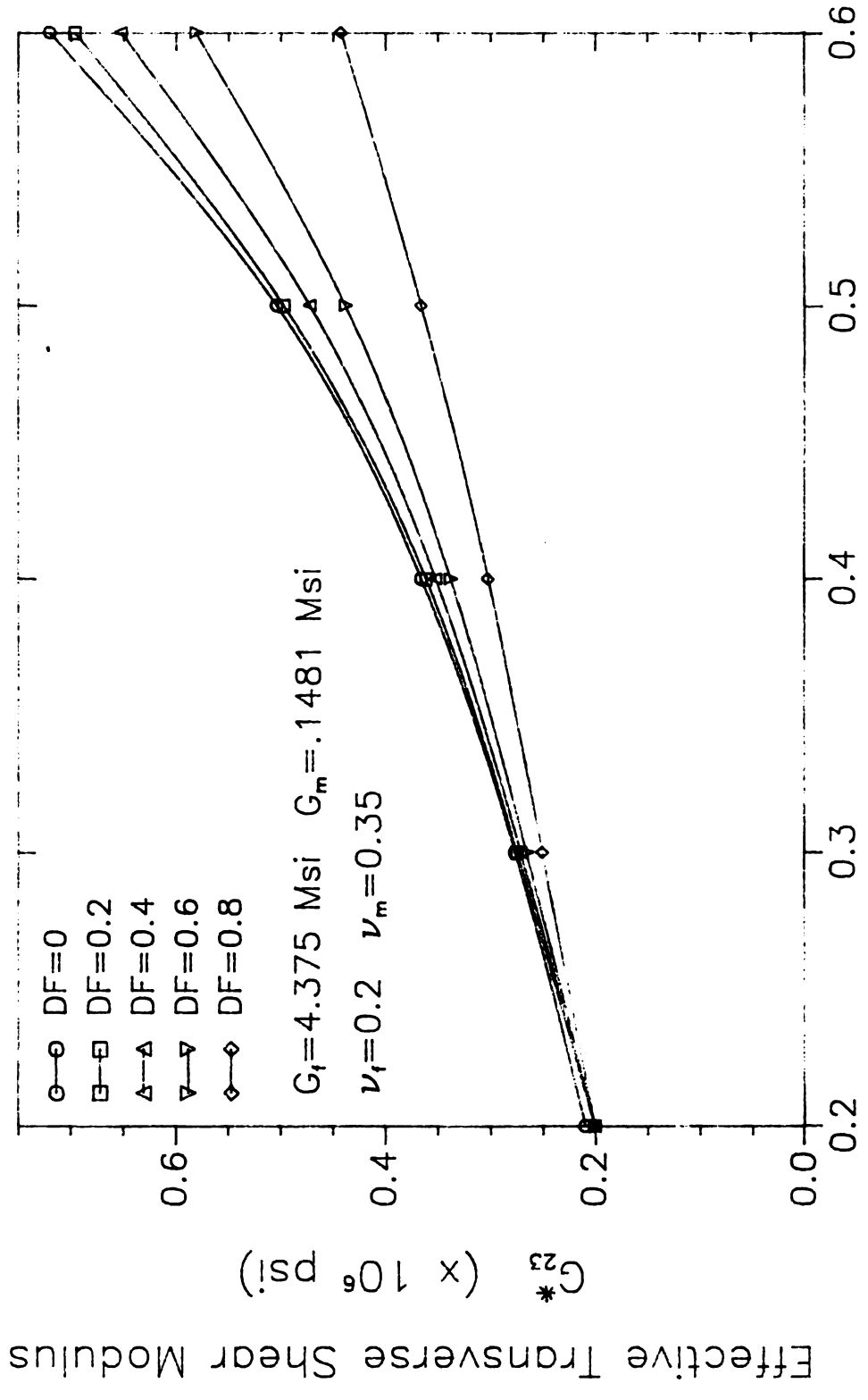

Figure 5.12. Effective transverse shear modulus G_{23}^* due to the degradation of interphase shear modulus G_m

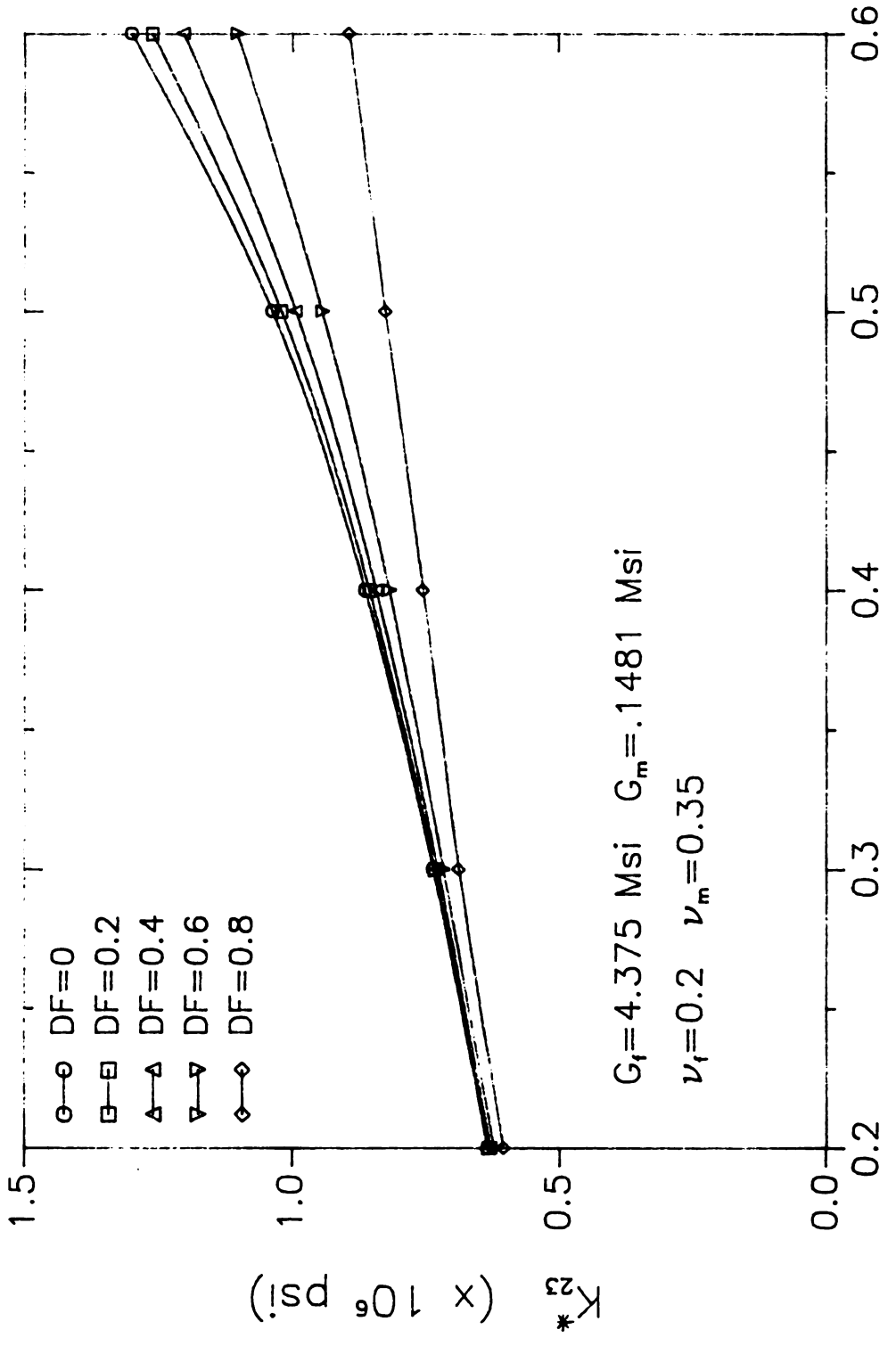

Figure 5.13. Effective plane strain bulk modulus K^*_{23} due to the degradation of interphase shear modulus G_m

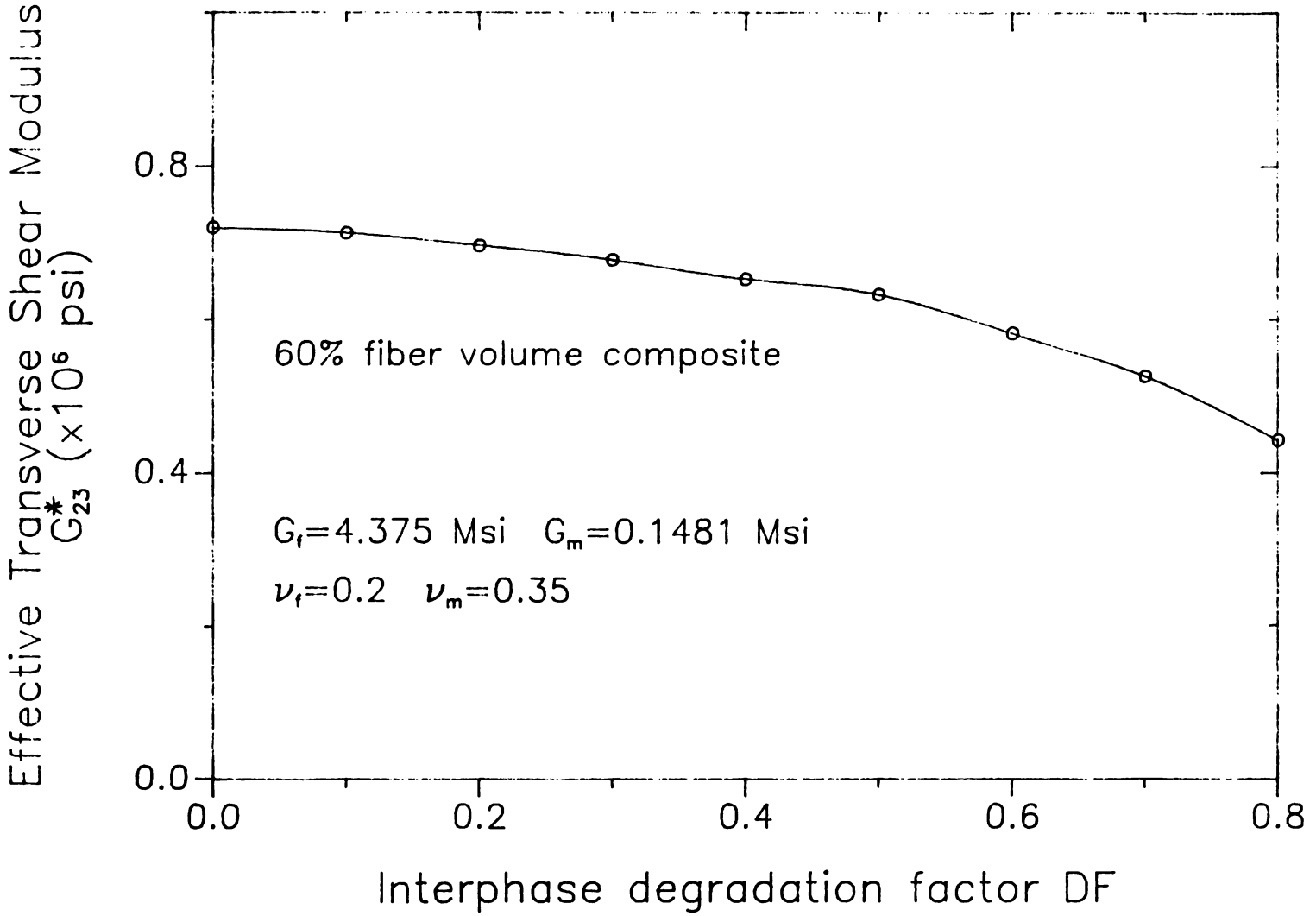

Figure 5.14. Influence of degradation factor DF on the effective shear modulus G_{23}^* at 60 % fiber volume composite

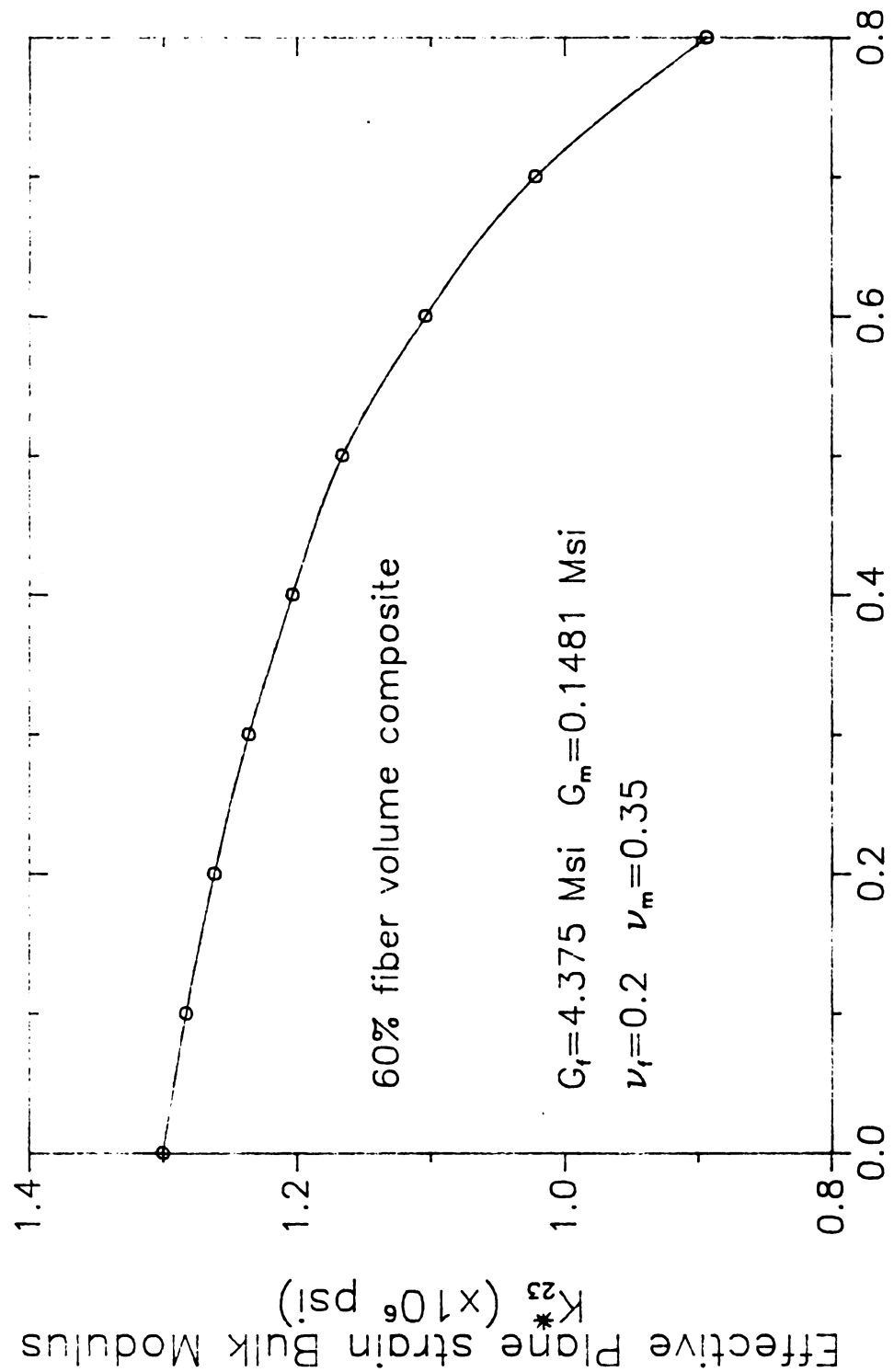

Figure 5.15. Influence of degradation factor DF on the effective plane strain bulk modulus K^*_{23} at 60 % fiber volume composite

Introduction of a tangential displacement discontinuity at the interface is another approach for examining the mechanical behavior of the damaged composite as described in equations (4.21 - 22). This model allows a jump of the tangential displacements at the fiber/matrix interface. If R = 0, one has a perfect interface bond. For $R \to \infty$, one has pure sliding at the interface. In the intermediate range ($0 < R < \infty$), it is very difficult to interpret the physical meaning associated to the behavior of the interface. The results are shown in the Figures 5.16 -19. The effective transverse shear modulus will be significantly decreased by an increase in R value. Specifically, for a certain R range ($0 \leq R \leq 5$), the reductions are dramatic. However, for $R \geq 50$, the decrease of the effective transverse shear modulus is steady. The plane strain bulk moduli remain the same as the perfect bond case for the entire range of R values. The reason may be that the shear stress at the fiber/matrix interface is much smaller than the normal stress due to the biaxial displacement boundary conditions, i.e. $u_2 = u_3 = u^0$.

In Table 5.6, the damaged effective plane strain bulk modulus and transversly shear modulus are listed for the interphase degradation model for the case of 60 percent fiber volume fraction.

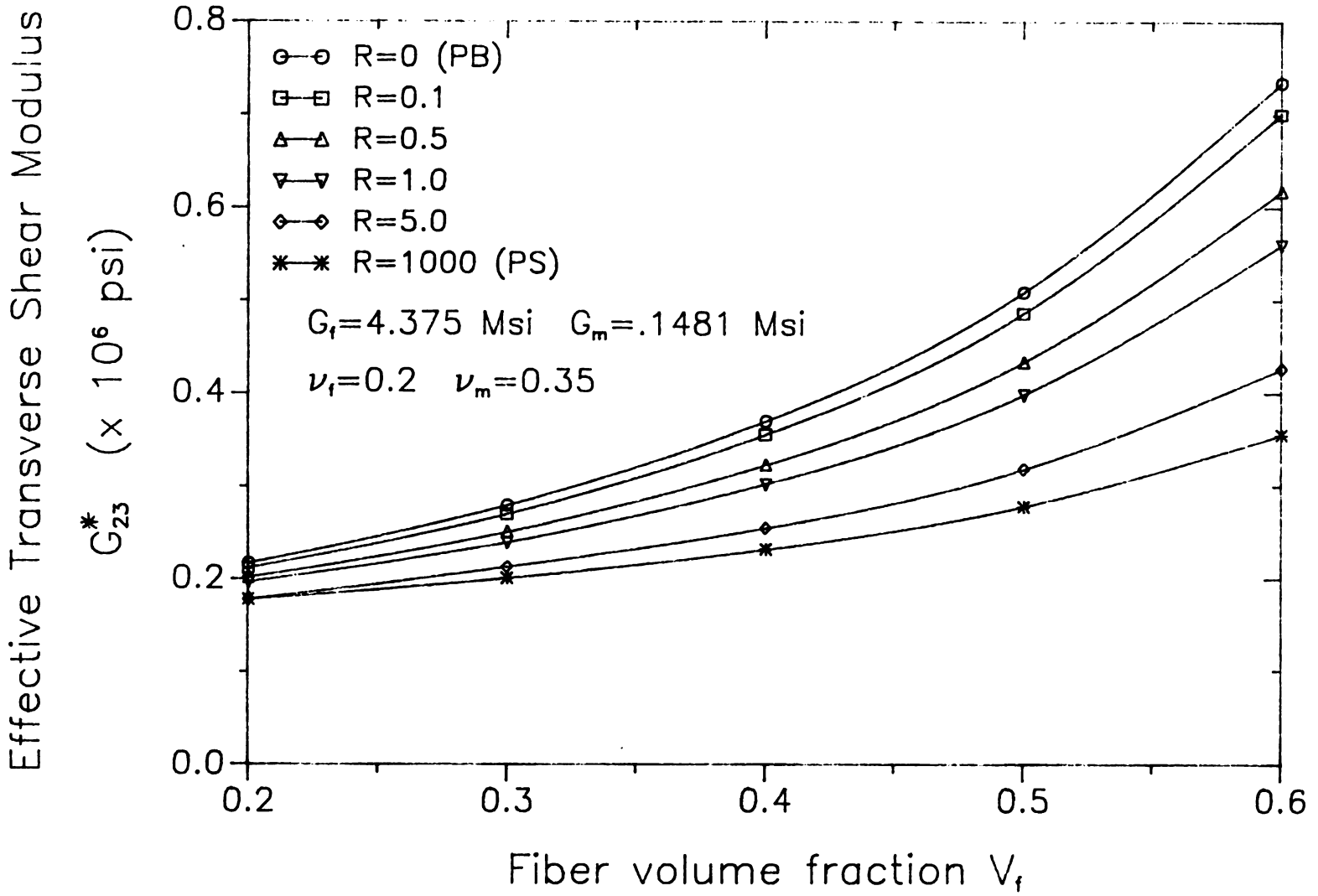

Figure 5.16. Effective transverse shear modulus G_{23}^* due to the tangential displacement discontinuity

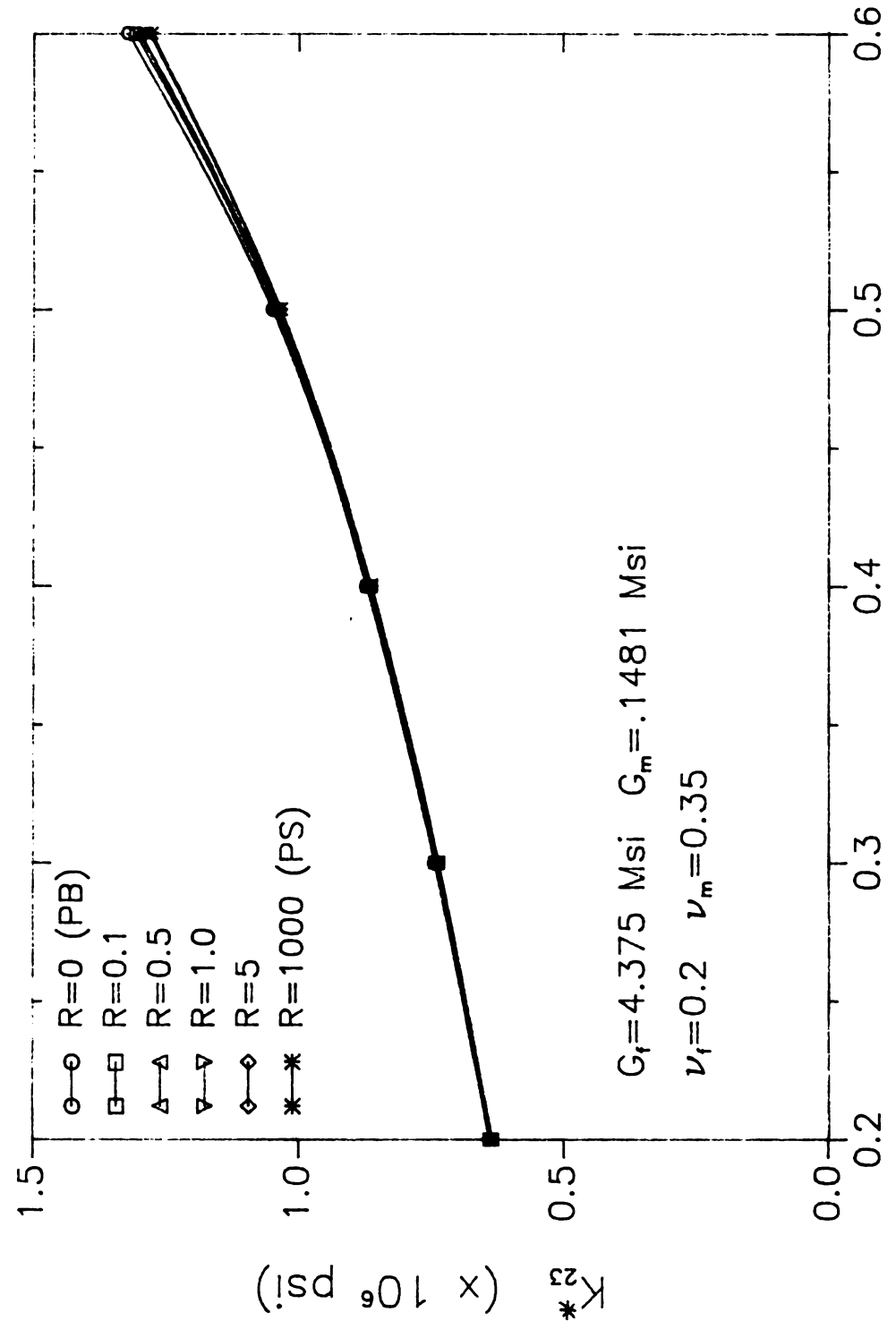

Figure 5.17. Effective plane strain bulk modulus K^*_{23} due to the tangential displacement discontinuity

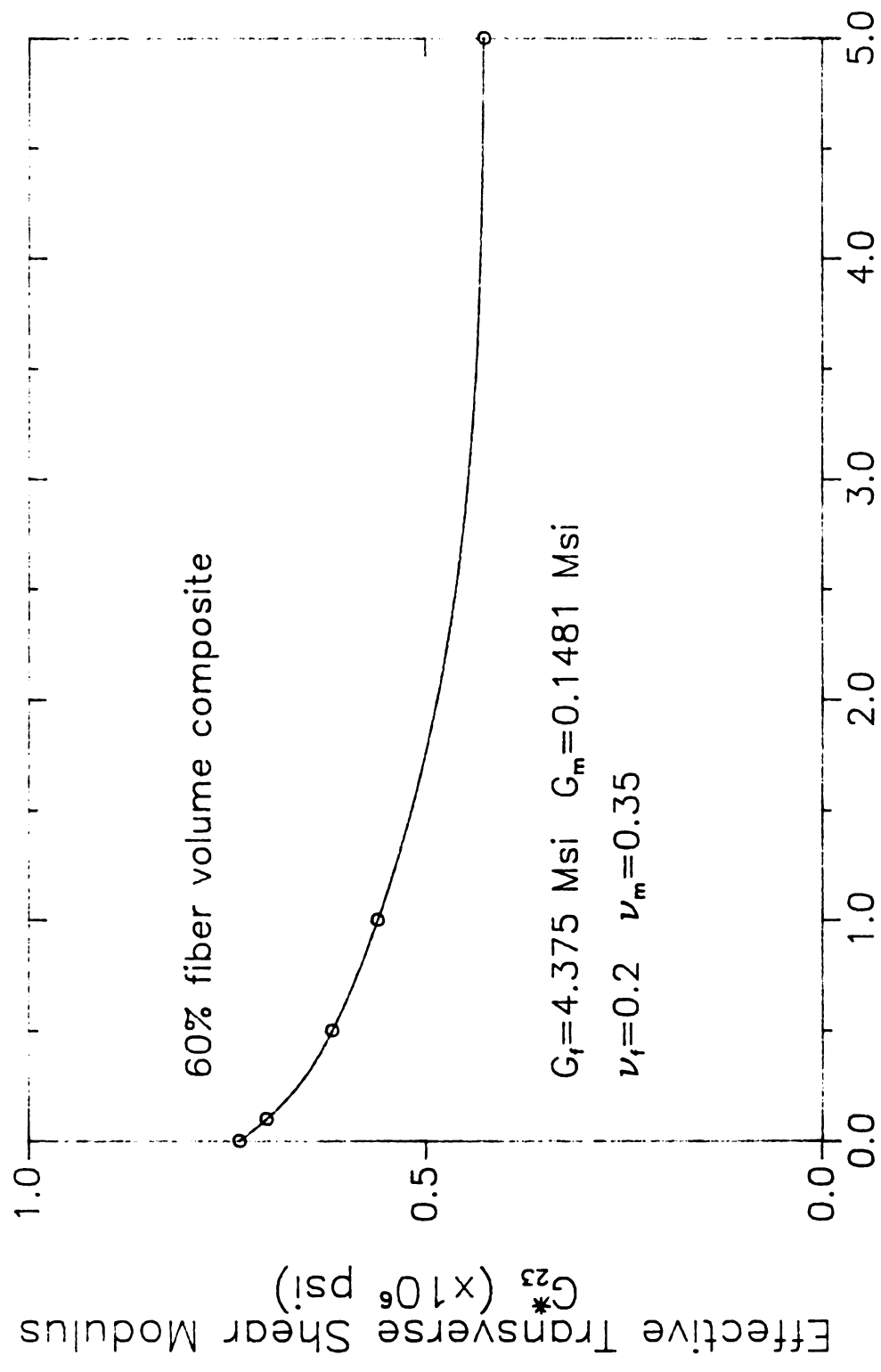

Figure 5.18. Influence of tangential displacement discontinuity factor R on the effective transverse shear modulus G_{23}^* at 60 % fiber volume composite

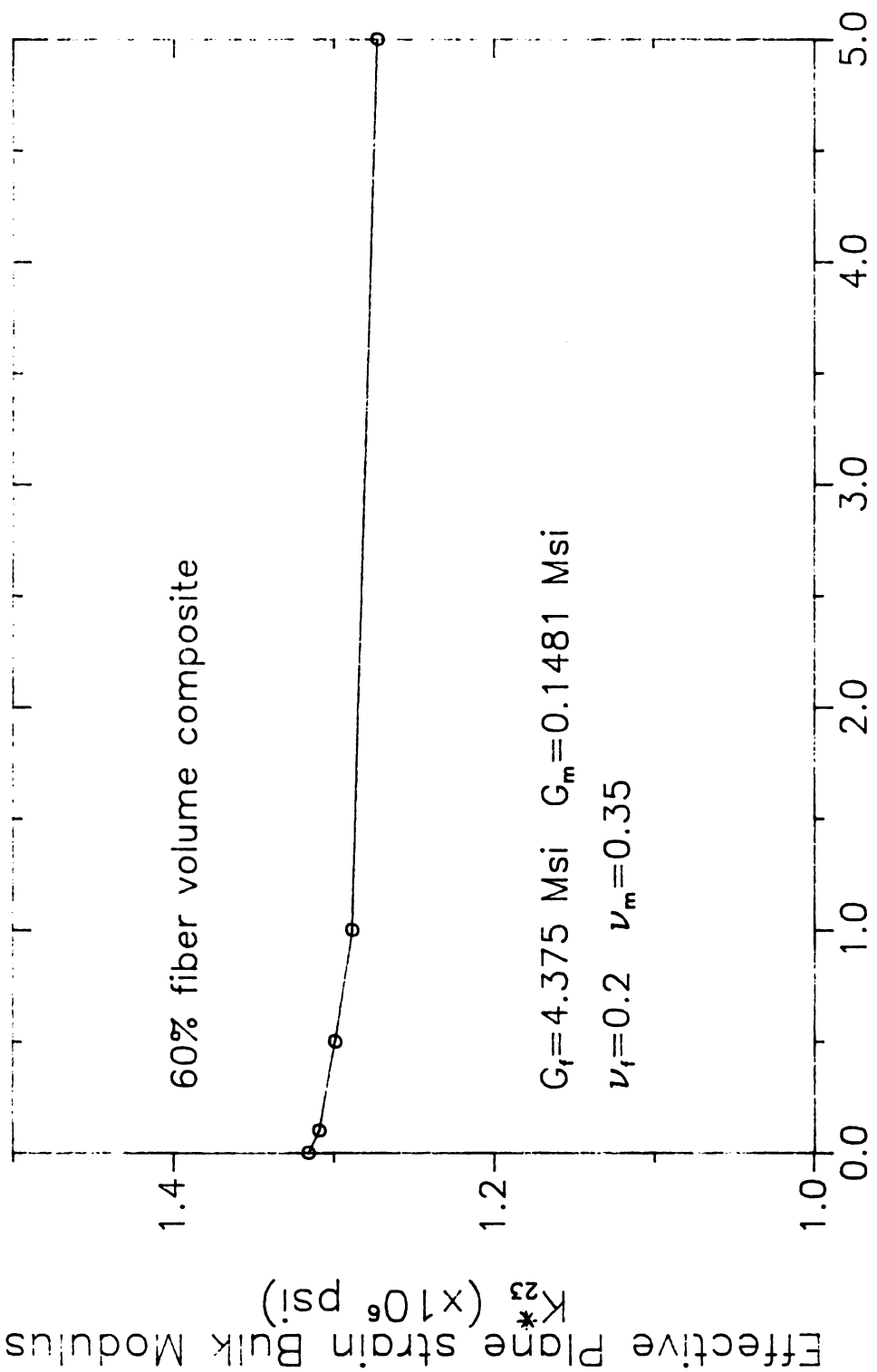

Figure 5.19. Influence of tangential displacement discontinuity factor R on the effective plane strain bulk modulus K^*_{23} at 60 % fiber volume composite

Table 5.6

Damaged effective plane strain bulk modulus and transversely shear modulus for the interphase degradation models at the $V_f = 0.6$.

unit = 10^6 psi

DF	G^*_{23}	K^*_{23}	DF	G^*_{23}	K^*_{23}
0.0	0.718	1.30	0.5	0.632	1.156
0.1	0.7126	1.282	0.6	0.581	1.103
0.2	0.696	1.262	0.7	0.525	1.021
0.3	0.6772	1.235	0.8	0.442	0.893
0.4	0.653	1.203			

CHAPTER 6

CONCLUSIONS AND RECOMMENDATIONS

A boundary element method has been presented for the analysis of thermally-induced residual stresses due to the cool-down process and effective transverse elastic properties for a transversely isotropic fiber-reinforced composite material. The square array of fibers as a fundamental unit has been applied to a number of problems and is in good agreement with other techniques.

The main advantage of this approach over other analytical techniques is its ability to handle interfiber effects and various fiber cross-sectional shapes. Furthermore, only the external boundary and interface needed to be discretized unlike the finite element technique. The numerical calculations were performed on a personal computer. In all problems, simple linear displacements and constant tractions on each element were used as shape functions for numerical treatment.

The main advantage of this work is its potential for modelling mechanical behavior of damaged interfaces in fiber-reinforced composites. If one measures micro-crack density κ at the fiber/matrix interface using non-destructive methods (e.g. acoustic emissions), the degradation of elastic properties of the interphase can be calculated. Then, with the present interphase degradation model, one can determine

the effective elastic properties of the fiber-reinforced composite material. Unlike the tangential displacement discontinuity method, this method gives a more physical meaning for a damaged or improperly bonded interfacial region.

Although axisymmetric and three-dimensional analyses have not been discussed here, it is felt that the method presented here could be extended to axisymmetric and three-dimensional micro-mechanics composite analysis without unreasonable difficilty. This extension will provide a full analysis of the effective elastic properties and thermally-induced residual stress distributions for composites.

BIBLIOGRAPHY

BIBLIOGRAPHY

1. Maxwel, J. C., Treatise on Electricity and Magnetism, 1st Ed., Clarendon Press, Oxford, 1873, p. 365

2. Lord Rayleigh, "On the influence of obstacles arranged in rectangular order upon the properties of a medium", Philosophical Magazine, Vol. 34, 1892, p. 481

3. Mura, T., Micro mechanics of Defects in Solids, Martinus Ninhoff, Hague, 1982

4. Voigt, W., "Über die beziehung zwischen den beiden elastizitätskonten isotroper körper", Wied. Ann., Vol. 38, 1889, p. 573

5. Reuss, A., "Berechnung der fliessgrenze uon mischkristallen auf grund der plastizitätsbedingung für einkristalle", Z. angew. Math. Mech., Vol. 9, 1929, p. 49

6. Hill, R., "The elastic behaviour of a crystalline aggregate", Proc. Physical Socity, London, Vol. A65, 1952, p. 349

7. Eshelby, J. D., "The determination of the elastic field of an ellipsoidal inclusion, and related problems", Proc. Roy. Soc., Vol. A241, 1957, p. 376

8. Kröner, E., "Berechnung der elastischen konstanten des vielkristalls aus den konstanten des einkristalls", Z. Phys., Vol. 51, 1958, p. 504

9. Budiansky, B., and Wu, T.T., "Theoretical prediction of plastic strains of polycrystals", Proc. 4th U.S. Nat. Congr. Appl. Mech., 1962, p. 1175

10. Hill, R., "Theory of mechanical properties of fiber-reinforced materials - I. elastic behaviour", J. Mech. Phys. Solids, Vol. 12, 1964, p. 199

11 Hashin, Z., "Assessment of the self-constistent scheme approximation: conductivity of particulate composites", J. Comp. Mater., Vol. 2, 1968, p. 284

12 Christensen, R. M. and Lo, K. H., "Solution for effective shear properties in three phase sphere and cylinder Models", J. Mech. Phys. Solids, Vol. 27, 1979, p. 315

13 Hashin, Z. and Shtrikman, "On some variational principles in anisotropic and nonhomogeneous elasticity", J. Mech. Phys.

Solids, Vol. 10, 1962, p. 335

14 Hashin, Z. and Shtrikman, "A variational approach to the elastic behaviour of multiphase materials", J. Mech. Phys. Solids, Vol. 11, 1963, p. 127

15 Hashin, Z. and Shtrikman, "A variational approach to the theory of the elastic behaviour of polycrystals", J. Mech. Phys. Solids, Vol. 10, 1962, p. 343

16 Hill, R., "Elastic properties of reinforced solids; some theoretical principles", J. Mech. Phys. Solids, Vol. 11, 1963, p. 347

17 Walpole, L. J., "On bounds for the overall elastic moduli of inhomogeneous systems - I", J. Mech. Phys. Solids, Vol. 14, 1966, p. 151

18 Walpole, L. J., "On bounds for the overall elastic moduli of inhomogeneous systems - II", J. Mech. Phys. Solids, Vol. 14, 1966, p. 289

19 Wu, T. T., "The effect of inclusion shape on the elastic moduli of a two-phase material", Int. J. solids and structures, Vol. 2, 1966, p. 1

20 Willis, J. R., "Bounds and self-consistent estimates for the overall properties of anisotropic composites", J. Mech. Phys. Solids, Vol. 25, 1977, p. 185

21 Kröner, E., "Bounds for disordered materials", J. Mech. Phys. Solids, Vol. 25, 1977, p. 137

22 Adams, D. F. and Doner, O. R., "Longitudinal shear loading of a unidirectional composite", J. Composite Materials, Vol. 1, 1967, p. 4

23 Adams, D. F. and Doner, O. R., "Transverse normal loading of a unidirectional composite", J. Composite Materials, Vol. 1, 1967, p. 152

24 Chen, C. H. and Cheng, S., "Mechanical properties of fiber reinforced composites", J. Composite Materials, Vol. 1, 1967, p. 30

25 Springer, S. G. and Tsai, S. W., "Thermal conductivities of unidirectional materials", J. Composite Materials, Vol. 1, 1967, p. 166

26 Gogól, W. and Furmański, P., "Some investigations of effective thermal conductivity of unidirectional fiber-reinforced composite", Enviromental Effects on Composite Materials, Vol. 2, Ed. Springer, Techomic Publishing, PA., 1984, p. 261

27 Lene, F. and Leguillon, D., "Homogenized constitutive law for a partially cohesive composite material", Int. J. solids structures, Vol. 18, 1982, p. 443

28 Benveniste, Y., "The Effective mechanical behaviour of composite materials with imperfect contact between the constituents", Mech. Materials, Vol. 4, 1985, p. 197

29 Mura, T., Jasiuk, I., Kouris D. and Furuhashi "Recent results of the equivalent inclusion method applied to composite materials", Composites '86 : Recent Advances in Japan and the United States proce. Japan-U.S. CCM-III, Tokyo, 1986, p.169

30 Jasiuk, I., Mura, T. and Tsuchida, E., "Thermal stresses and thermal expansion coefficients of short fiber composites with sliding interfaces", J. Eng. Mater. Technology, Vol. 110, 1988, p. 96

31 Mori, T. and Tanaka, K., "Average stress in matrix and average energy of materials with misfitting inclusions", Act. metall., Vol. 21, 1973, p. 517

32 Dundurs, J. and Zienkiewicz, O. C., "Stresses around circular inclusions due to thermal gradients with particular reference to reinforced concrete", J. Amer. Concrete Inst., 1964, p. 1523

33 Sternberg, E. and McDowell, E. L., "On the steady-state thermoelastic problem for the half-space", Quart. Appl. Math., Vol. 14, 1957, p. 381

34 Tauchert, T. R., "Thermal stress concentrations in the vicinity of cylindrical inclusions", J. Composite Materials, Vol. 5, 1970, p. 868

35 Hecker, S. S., Hamilton, C. H. and Ebert, L. J., "Improved fiber composite tensile performance by mechanical residual stress relief", Transactions Quart. ASMQA, Vol. 62, 1969, p. 740

36 Sachs, G. and Espey, G., "Residual stresses in metals", Iron Age, Vol. 128, 1941, p. 63

37 Hecker, S. S., Hamilton, C. H. and Ebert, L. J., "Elastoplastic analysis of residual stresses and axial loading in composite cylinders", J. Materials, JMLSA, Vol. 5, 1970, p. 868

38 Hoffman, C. A., "Effects of thermal loading on fiber-reinforced composites with constituents of differing thermal expansivities", J. Eng. Mater. Technology, Vol. 95, 1973, p. 55

39 Miller, A. K. and Adams, D. F., "Inelastic micromechanical analysis of graphite/epoxy composites subjected to hygrothermal cycling", ASTM STP 658, 1978, p. 121

40 Uemura, M., Iyama, H. and Yamaguchi, Y., "Thermal residual

stresses in filament-wound carbon-fiber-reinforced composites", J. Thermal Stresses, Vol. 2, 1979, p. 393

41 Weitsman, Y., "Residual thermal stresses due to cool-down of epoxy-resin composite", J. Appl. Mech., Vol. 46, 1979, p. 563

42 Herrmann, K. and Matteck, K., "Thermal stresses in the unit cell of a fiber-reinforced Material", J. Thermal Stresses, Vol. 2, 1979, p. 15

43 Rohwer, K. and Jiu, X., "Micromechanical curing stresses in CFRP", Composite Science and Technology, Vol. 25, 1986, p. 169

44 Avery, W. B. and Herakovich, C. T., "Effect of fiber anisotriopy on thermal stresses in fibrous composites", J. Appl. Mech., Vol. 53, 1986, p. 751

45 Adams, D. F., "A Micromechanics analysis of the influence of the interface on the performance of polymer-matrix composites", J. Reinforced plastics and composites, Vol. 6, 1987, p. 66

46 Vedula, M., Pangborn, R. N. and Queeney, R. A., "Fiber anisotropic thermal expansion and residual thermal stress in a graphite/aluminium composite", Composites, Vol. 19, 1988, p. 55

47 Vedula, M., Pangborn, R. N. and Queeney, R. A., "Modification of residual thermal stress in a metal-matrix composite with the use of a taileres interfacial region", Composites, Vol. 19, 1988

48 Hahn, H. T. and Kim, K. S., "Hygroscopic effects in aramid fiber/epoxy composite". J. Eng. Mater. Technology, Vol. 110, 1988, p. 153

49 Rich, M. and Drzal, L. T., "Interfacial properties of some high-strain carbon fibers in an epoxy matrix", J. Reinforced plastics and composites", Vol 7, 1988, p. 145

50 Sideridis, E., "The in-plane shear modulus of fiber reinforced composites as defined by concept of interphase", Composite Science and Technology, Vol. 31, 1988, p. 35

51 Davidge, R. W. and Green, T. T., "The strength of two-phase ceramic/glass materials", J. Materials Science, Vol. 3, 1968, p. 629

52 Evans, A. G. and Fu, Y., "Some effects of microcracks on the mechanical properties of brittle solids - II", Acta Metall., Vol. 33, 1985, p. 1525

53 Lange, F. F., "Fracture of brittle matrix, particulate composites", Composite Materials Vol.5, Ed. Broutman, Academic Press, 1974

54 Rubinstein, R. and Fitzgerald, J. E., "Further developments of a

damage theory for filled polymers", Polymer Eng. Science, Vol. 19, 1979, p. 151

55 Danson, D., "Linear isotripic elasticity with body forces", Progress in Boundary Element Method, Vol. 2, Ed. Brebbia, Pentech press, 1983

56 Cruse, T. A., "Boundary-integral equation method for three-dimensional elastic fracture mechanics analysis", AFOSR-TR-75-0813, 1975

57 Brebbia, C. A., The Boundary Element Method for Engineers, Pentech press, London, 1978

58 Lachat, J. C., "A further development of the boundary integral technique for elastostatics", Ph.D Thesis, University of Southampton, 1975

59 Rizzo, F. J., "An integral equation approach to boundary value problems of classical elastostatics", Quart. Appl. Math. Vol. 25, 1967, p. 83

60 Riccardella, P. C., "An implementation of the boundary-integral technique for planar problems of elasticity and elastoplasticity", Report No. SM-73-10. Department of Mechanical Engineering, Carnegie Mellon University, 1973

61 Kumar, V. and Mukherjee, S., "A boundary integral equation formulation for time-dependent inelastic deformation in metals", Int. J. Mech. Sci., Vol. 19, 1977, p. 713

62 Mukherjee, S. and Ghosh, S., "Boundary element method analysis of thermoelastic deformation in nonhomogeneous media", Int. J. solid structures, Vol. 20, 1984, p. 829

63 Sur, U., "A numerical method for the treatment of kanked cracks in finite bodies", Ph.D Thesis, Michigan State University, 1987

64 Haenerr, J. and Ashbaugh, N., "Three-dimensional stress distribution in a unidirectional composite", J. Composite Materials, Vol. 1, 1967, p. 54

65 Hashin, Z., "Analysis of properties of fiber composites with anisotropic constituents", J. Appl. Mech., Vol. 46, 1979, p. 543

66 Benedetto, A. T. and Nicolais, L., " Advances in composite materials", Ed. Piatti, Applied Science Publishers, p. 153

67 Binns, D. B., "Science of Ceramics", Ed. Steward, Vol. 1, Academic press, NY, 1962, p. 315

68 Venturini, W. S. and Brebbia, C. A., "Application in geomechanics", Topics in Boundary Element Research, Ed. Brebbia, Springe-Verlag, Vol. 1, 1984

69 Walsh, J. M., J. Geophys. Res. Vol. 70, 1965, p. 399

70 Fitzgerald, J. E. and Rubinstein, R., "Metatropic material : a theory for permament memory effects", Report AFOSR-72-2322, 1976

71 Adams, D. F., "Influence of the polymer matrix on the mechanical response of a unidirectional composite", Progress in Science and Engineering of Composites Vol. 1, ICCM-IV, 1982, p. 507

72 Koufopoulos, T. and Theocaris, P. S., "Shrinkage stresses in tao-phase materials", J. Composite Materials, Vol. 3, 1969, p. 308

73 Hsu, T. T., "Mathematical analysis of shrinkage stresses in a model of hardened concrete", Proc. Amer. Concr. Inst., Vol. 60, 1963, p.371

74 Christensen, R. M., Mechanics of Composite Materials, 1979, John Wiley & Sons, New York

75 Laws, N., "Composite materials : Theory vs. Experiment", J. Composite Materials, Vol. 22, 1988, p. 396